MASTER'S THESIS

A computational study of energy conversion efficiency of F1-ATPase

Zou, Yazhong

Date of Award:
2017

HONG KONG BAPTIST UNIVERSITY

Master of Philosophy

THESIS ACCEPTANCE

DATE: September 21, 2017

STUDENT'S NAME: ZOU Yazhong

THESIS TITLE: A Computational Study of Energy Conversion Efficiency of the F_1-ATPase

This is to certify that the above student's thesis has been examined by the following panel members and has received full approval for acceptance in partial fulfillment of the requirements for the degree of Master of Philosophy.

Chairman:	Prof. Wong Ricky N S Chair Professor in Biology, Department of Biology, HKBU (Designated by Dean of Faculty of Science)
Internal Members:	Prof. Van Hove M. A. Head, Department of Physics, HKBU
	Prof. Tang Lei Han Professor, Department of Physics, HKBU
External Members:	Prof. Ching Shuk Chi Emily Professor Department of Physics The Chinese University of Hong Kong

Issued by Graduate School, HKBU

A Computational Study of Energy Conversion Efficiency of F_1-ATPase

ZOU Yazhong

A thesis submitted in partial fulfillment of the requirements

For the degree of

Master of Philosophy

Principal Supervisor:

Prof. TANG Lei Han (Hong Kong Baptist University)

September 2017

DECLARATION

I hereby declare that this thesis represents my own work which has been done after registration for the degree of MPhil at Hong Kong Baptist University, and has not been previously included in a thesis or dissertation submitted to this or any other institution for a degree, diploma or other qualifications.

I have read the University's current research ethics guidelines, and accept responsibility for the conduct of the procedures in accordance with the University's Committee on the Use of Human & Animal Subjects in Teaching and Research (HASC). I have attempted to identify all the risks related to this research that may arise in conducting this research, obtained the relevant ethical and/or safety approval (where applicable), and acknowledged my obligations and the rights of the participants.

Signature: 郭亚中

Date: September 2017

ABSTRACT

ATP synthase (F_1F_O-ATPase) is an essential enzyme for life. Powered by an electrochemical proton gradient, it catalyzes ADP and phosphate into ATP. The F_1-subunit of ATP synthase is called F_1-ATPase as it also independently catalyzes the reverse reaction in absence of F_O-part. The nearly 100% energy conversion efficiency of the molecular motor has attracted the attention of many physicists and biologists to explore the underlying thermodynamics. Recently, a new nonequilibrium equality derived by Harada and Sasa (Harada & Sasa, 2005) was applied to the experimental time series data on F_1 -ATPase to extract heat flow to the environment. A phenomenological model for rotary motion was proposed and shown to reproduce key experimental features. Interested in the high efficiency of F_1-ATPase and the good performance of the corresponding model, we carried out a detailed computational study of the model to understand its behavior in a broader range of parameter values. We solved the model using a modified Gillespie algorithm for stochastic simulation and by integrating the Fokker-Planck equation. Various physical properties of the model, such as the relation between rotational velocity and parameters characterizing angular dependence (q) and ATP switching rates (W), the relation between two kinds of dissipation and rotational velocity, the negative heat flow from environment to system through ATP binding etc. are analyzed in detail. Importantly, we modified the driving potential to investigate the factors affecting the efficiency. Additionally, we found some inconsistences between properties of this model and previous studies and we could unify them by some adjustments, which may be useful for constructing more precise models in the future.

ACKNOWLEGMENTS

First and foremost, I would like to offer my sincere appreciation to my supervisor, Prof. TANG Lei-han for the inspirations and supports in my postgraduate period. He is a talented physicist who can bring me into a splendid physical world. Besides, his push stimulates my potential for deeper knowledge and harder challenges.

Secondly, I sincerely appreciate the help from senior students, Dr. WANG Shouwen, Dr. TANG Qianyuan, Qi Fei and WANG Yang who offered me plenty of kind help with patience.

Thirdly, I have to thanks all my dear friends acquainted in Beijing when I was a bachelor. Even I come to Hong Kong, they still payed visits to me frequently and provided me with infinite help, guide and comfort, accompanying me in hard time. Besides, all new friends I met in Hong Kong and Shen Zhen helped me a lot in my postgraduate life.

Last but not the least, I would like to thank my family for their support to my bravery tries.

TABLE OF CONTENTS

LIST OF FIGURES

LIST OF ABBREVIATIONS

TASAM: The Totally Asymmetric Allosteric Model

HSE: Harada and Sasa equality

HFSE: Heat flow between the system and the environment

FT: Fluctuation Theorem

1. Introduction and thesis Outline

1.1 The F_1F_0-ATPase

ATP synthase is an essential molecular motor that produces the energy storage molecule adenosine triphosphate (ATP). ATP is the most commonly used "energy currency" in cells from bacteria to human beings, and it is synthesized from ADP and phosphate (P_i). The process of ATP synthesis is driven by the electrochemical gradient of proton (H+).

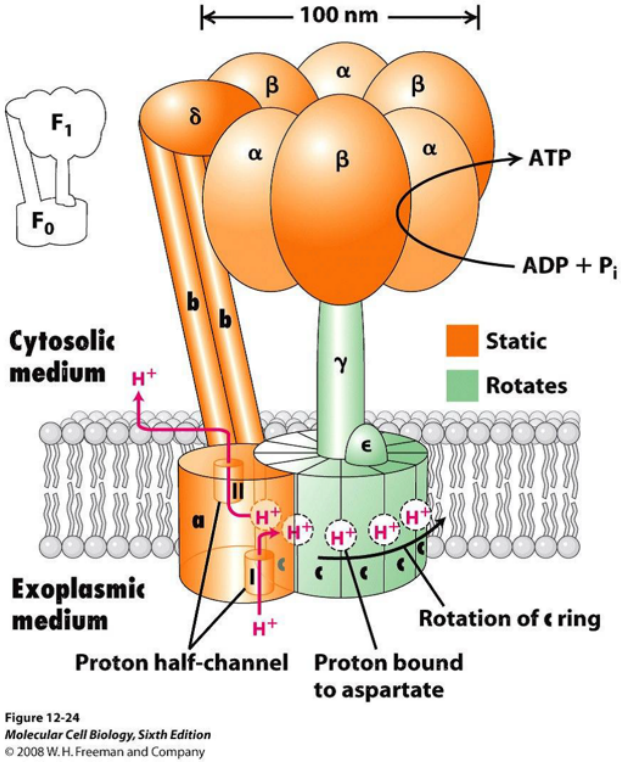

Figure 1-1 ATP synthase (Lodish, 2008)

ATP synthase is embedded between the inner mitochondrial membrane and the thylakoid membrane in eukaryotic cells or the plasma membrane in bacteria. In plant, it is also found in the thylakoid lumen through the thylakoid membrane and into the chloroplast for photosynthesis It can be separated into two components as shown in Figure 1-1. The F_O part is located within the membrane, while the F_1 part which carries out the catalytic function is outside the membrane (Junge & Nelson, 2015; Daichi Okuno, Iino, & Noji, 2011).

The core complex of the F_1 portion is a hexamer which is composed of 3 $\alpha\beta$-dimers arranged around the central γ, δ and ϵ units. It is a rotary molecular machine that can not only catalyse ADP and P_i into ATP when the F_O portion is present but also hydrolyse ATP when run in the reverse direction, so the F_1 portion is also named F_1-ATPase.

1.2 The mechanochemical coupling of F_1F_O-ATPase

From 1960s to 1970s, Paul Boyer developed the binding-change model, which proposed that the ATP catalytic reaction is relied on the conformational change of the core complex of F_1 portion induced by rotation of the γ subunit (Boyer & Kohlbrenner, 1981), in other words, the coupling is mechanical. In his model, F_O is a motor driven by the proton gradient while F_1 is another motor driven by ATP hydrolysis and they are connected to each other by a bar-like shared portion, γ unit. The reversible reaction and binding-change model lead to opposite motions for opposite reaction directions of ATP synthase.

If the protons flow from the bottom to the top as shown in Figure 1-1, the γ will rotate in counter-clockwise from the top view, and the electric potential energy will be converted into chemical free energy. On the other hand, when the amount of ATP is rich, the ATP will be hydrolyzed by F_1 and therefore, chemical energy will be transduced into mechanical energy and then, the electric potential energy accompanied with clockwise γ rotation and downward protons flow. He suggested that two kinds of energy will compete with each other and corresponding reactions and motions follow. Later studies show that the coupling is tight (Adachi et al., 2000; Yasuda, Noji, Kinosita, & Yoshida, 1998), which means each step of a rotation is tightly driven by the hydrolysis of one ATP.

Then, John Walker and his collaborators determined the DNA sequences of genes encoding the proteins in the ATP synthase. The first X-ray structure of F_1 indicated that the binding-change mechanism proposed by Boyer was correct. In 1997, the Nobel prize in chemistry was awarded to Paul D. Boyer and John E. Walker for their elucidation of the enzymatic mechanism underlying the synthesis of ATP.

1.3 High frequency measurement of rotary motion

The unique mechanochemical mechanism of the ATP synthase has attracted detailed investigations of its dynamics over the years (Adachi, Oiwa, Yoshida, Nishizaka, & Kinosita, 2012; Rikiya Watanabe et al., 2011). Studies have shown that ATP synthase converts chemical energy into mechanical one with nearly 100% efficiency, which is particularly intriguing to biophysicists and statistical physicsist.

The high temporal resolution data revealed two main sub-steps and two dwells in one ATP hydrolysis reaction cycle catalysed by the core complex $\alpha_3\beta_3$ of the F_1 Portion (Sugawa et al., 2016). Firstly, the catalytic site in β subunit needs to wait for an ATP to bind, and this dwell is called ATP waiting dwell. Then, the product ADP is released before the first 80° rotation. The affinity change of ADP implies that ADP release benefits part of the energy to enable the first rotation while ATP binding energy contributes most of it. Following the above description, the catalytic sub-step which is made of two rate-limiting steps, one is ATP cleavage and another is release of the product P_i. The 40°rotation is followed. In the latter process, the decreased affinity of P_i drives the motor to rotate. The angle-dependent mechanically driven ATP hydrolysis by F1-ATPase has been carefully studied by a number of research groups (Adachi et al., 2007; Nishizaka et al., 2004; Shimabukuro et al., 2003; Sugawa et al., 2016; Yasuda, Noji, Yoshida, Kinosita, & Itoh, 2001). The whole hydrolysis reaction is depicted below:

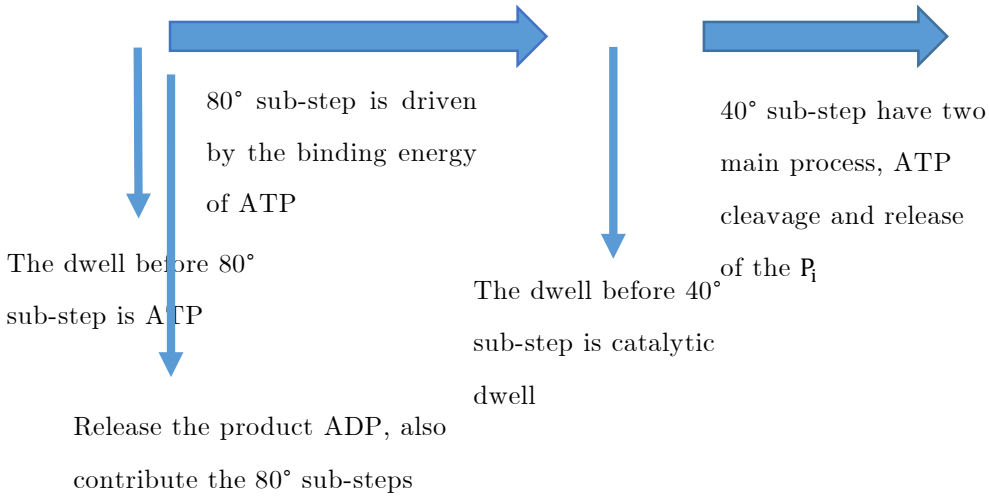

Figure 1-2 Hydrolysis reaction flow chart

we refer to the details of the experiment in chapter 2.

1.4 Theoretical studies of the energy conversion efficiency

Theoretical developments on stochastic thermodynamics, where fluctuations are significant comparing to macroscopic systems (Reimann, 2002; Sekimoto, 2010), have provided the tools to investigate molecular motors with new perspectives (Horowitz, Sagawa, & Parrondo, 2013). Data from the high-speed microscopic measurement (Toyabe et al., 2010) led to the construction of models (Kyogo Kawaguchi, Sasa, & Sagawa, 2014) that allow detailed investigation of the energy dissipation process which has a relation on the rate of energy dissipation and an extent of the fluctuation-response relation violation (Harada & Sasa, 2005), have been built to investigate the high efficiency of ATP synthase.

Molecular motors are in the size of nanometers, where the thermal fluctuation play an important role on them, so they exhibit stochastic dynamics and energetics. For the same reason, molecular motors are usually described by Langevin, Fokker-Planck and master equations (Zimmermann & Seifert, 2012).

A crucial problem under fluctuation world is how to define the efficiency of these stochastic systems. Actually, there are different kinds efficiencies can be defined based on whether we concentrate on the work against an external force or work against viscous friction (Boksenbojm & Wynants, 2009; Derényi, Bier, & Astumian, 1999; M. Qian, Zhang, Wilson, & Feng, 2008; Seifert, 2013; Suzuki & Munakata, 2003; H Wang, 2005; Hongyun Wang & Oster, 2002).

In experiments, the motion of molecular motors is not observed directly. Instead, the trajectory of the probe attached to the motor protein is recorded and analysed. In addition, an external force can be applied on the probe to control the motors by controlling the probes (Itoh, Takahashi, Adachi, & Noji, 2004; Noji, Yasuda, Yoshida, & Jr, 1997).

The elastic linker between the probe and molecular motor may introduce a delay in the coupling (Bouzat & Falo, 2010; H Wang & Zhou, 2008), but since all the experiments we referenced do not take this into account, we just treat the trajectory of probes as the rotation of γ subunit and assume the delay between the probe and γ would not affect the dynamics of F_1-ATPase.

Now, according to the energy transduction which we will discuss in the next chapter, we focus on two different definitions of efficiency that commonly used for motor proteins. We can compare the energy dissipates from the probe to the consumed chemical energy $\Delta\mu$. The ratio can be described by

$$\eta_Q \equiv \frac{Q_{ext}}{\Delta\mu} \tag{1.1}$$

where Q_{ext} stands for the heat dissipation from the probe. This efficiency does not have to be smaller than 1 and has been discussed earlier (Kinosita, Adachi, & Itoh, 2004; Hongyun Wang & Oster, 2002). In this way, we also call η_Q a pseudo efficiency.

Another kind of efficiency is the Stokes efficiency, which is the ratio of the work against drag force $\Gamma v_s^2/3v_s$ and the chemical free energy

$$\eta_S \equiv \frac{\Gamma v_s}{3\Delta\mu} \tag{1.2}$$

here, the Γ is the rotational fraction coefficient in *vivo* solution and v_s represents the mean rotational velocity of the molecular motor. In contrast to the pseudo efficiency, the Stokes efficiency is bounded by 1 (Hongyun Wang & Oster, 2002).

1.5 Organization of the thesis

In this chapter, we have introduced the biological structure of F_1F_O-ATPase and the mechanochemical mechanism with sub-steps scheme chart. Plus, we have introduced two types of efficiencies commonly used in stochastic systems. The experiments of using different methods will be reviwed in the next chapter and we will do preliminary discussion about their results. In chapter 3, we will present the stochastic model of F_1-ATPase and the details of simulation, furthermore, we will compare our results with the original model. In chapter 4, we will demonstrate the results of simulation and explain the details about every quantity obtained. In chapter 5, we will analyse the energy conversion efficiency combined with experiments of wild type, then try to figure out and prove the properties we found by designing the mutants of the above model, which are allowed experimentally. In the end, we will discuss the reasons we obtained about the energy conversion efficiency and the disagreements we met among theories and experiments.

2. Review of Experiments

Due to the improvements in experiments, the motion of a single molecular motor and its trajectories can be recorded with higher and higher temporal and spatial resolutions. Since the first time the rotary motion of F_1-ATPase has been observed in experiment (Noji et al., 1997), of which there are number of different methods have been applied to measure the efficiency. Then, we will demonstrate the energy flow for the ATP hydrolysis reaction and briefly introduce four types of experiments with different theories or methods.

2.1 The energy transduction

In the previous chapter, we have introduced details of hydrolysis reaction of F_1-ATPase, and the heat flow can be shown as bellow

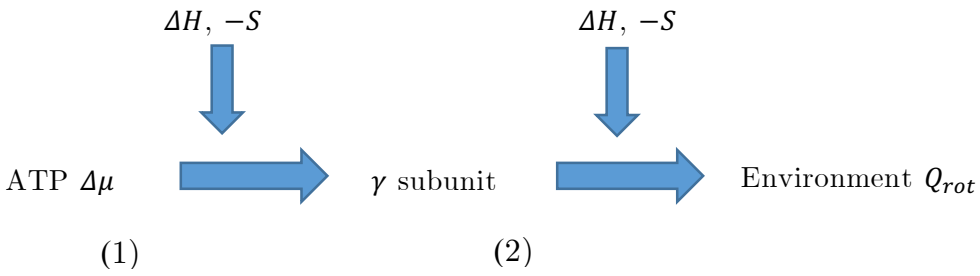

Figure 2-1 The heat flow of F_1-ATPase

The energy transduction can be simplified as (1) and (2) steps in Figure 2-1. Firstly, the chemical free energy of an ATP $\Delta\mu$ is injected to the F_1motor through binding. Then, the chemical energy is transformed into mechanical energy of γ subunit and $\alpha_3\beta_3$ complex, and finally, the energy would dissipate through the motion of probe, either in steady unidirectional motion or fluctuation motion.

Due to the nonequilibrium nature of the cycle, heat exchange with the environment in step (1) and (2) can be positive and negatve (G. M. Wang, Sevick, Mittag, Searles, & Evans, 2002)

Although many of studies (Kinosita, Yasuda, Noji, & Adachi, 2000; George Oster & Wang, 2000; Toyabe & Muneyuki, 2013; Toyabe, Watanabe-Nakayama, Okamoto, Kudo, & Muneyuki, 2011; Yasuda et al., 1998, 2001) claimed the Stokes efficiency is nearly 100% (both (1) and (2) steps), both the experiment and the model of recent works (Kyogo Kawaguchi et al., 2014; Toyabe et al., 2010b) state that the 100% efficiency applies only to step (1) shown in above figure. The stokes efficiency in step (2) may require more careful definition.

2.2 Four experiments and previous data analysis

Before introducing specific experiments, we introduce the common set up and methods first. The F_1 part is isolated and adhers to a glass surface. A probe or a filament is attached to the γ subunit in order to observe its motion under optical microscopes as shown in **a** of Figure 2-2.

After the protein having been set up, one can observe and record the motions of the probe under varying substrates concentration or apply external force through the probe. The right panel in Figure 2-2 shows examples of trajectories under different external applied torques, where Y axis stands for the rotary angle from 0° and X axis represents the time. Nearly all methods introduced below use the trajectories to calculate the quantities of interest. Then we will introduce four experiments in the order of the time they published.

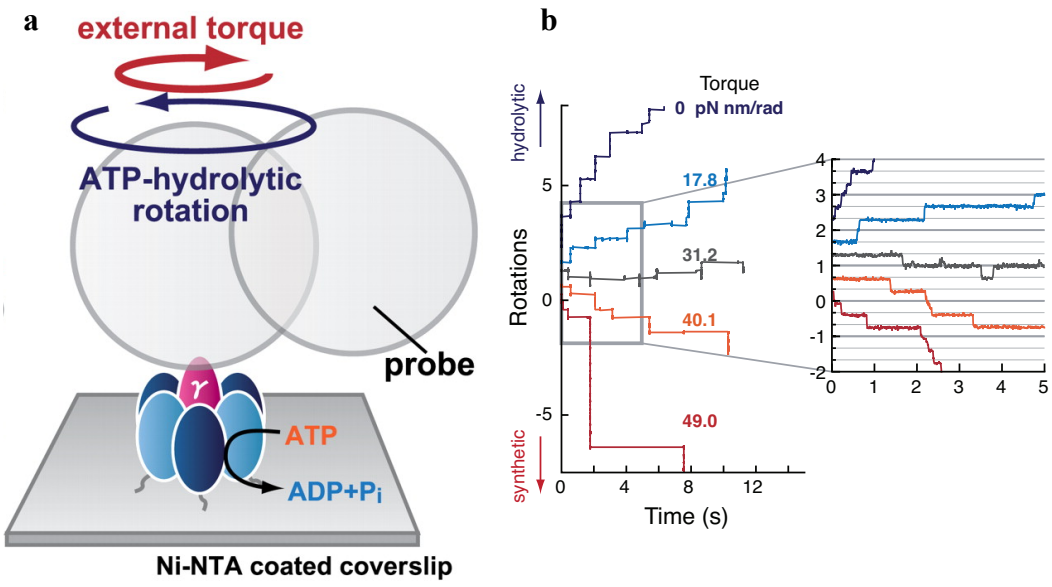

Figure 2-2 The common setup of experiments and examples of motion trajectories (Toyabe et al., 2011)

2.2.1 The direct analysis from trajectories

The experiment done by Yasuda et al. not only revealed the 90°(80°) and 30°(40°) sub-steps of the 120° step but also show the motor produces a constant torque upon each ATP binding/hydrolysis event as expected in a previous study (Yasuda et al., 1998). The torque observed during the 120° rotation is nearly independent of rotation angle and ATP concentration in nM − mM range. The work that is calculated according to the torque in each rotation event is nearly the same as the free energy of ATP, $\Delta\mu$, indicating the Stokes efficiency $\eta_S \approx 100\%$. The torque they obtained is directly calculated from the trajectories and the method can be briefly described below

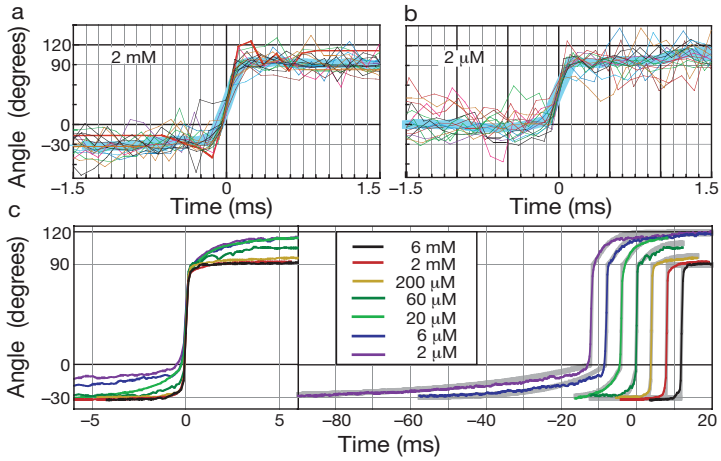

Figure 2-3 The direct analysis from trajectories (Yasuda et al., 2001)

As **a** and **b** shown in Figure 2-3, firstly, they superimposed and averaged trajectories under specific ATP concentration, obtaining the averaged angle-time lines (thick cyan line). Then, they calculate the rotational velocity-time diagrams under varying ATP concentration. Finally, the torque-time diagrams is obtained by the Stokes' law. We can observe by eyes in **c** that the rotary time from 0° to 90° from 2μM to 6mM is nearly the same and quite short.

2.2.2 Calculating the rotary dissipation by HSE

Looking deep into the energy dissipation from the probe to the environment, the probe feels a force of $-\Gamma v(t) + \xi(t)$ from the environment, where $\xi(t)$ is the random force due to the thermal fluctuation and theoretically, the heat dissipation rate can be defined as $J \equiv \langle[\Gamma v(t) - \xi(t)]v(t)\rangle$, where $\langle \dots \rangle$ represents the ensemble average. However, the random force cannot be measured in experiments. Recently, an equality derived by Harada and Sasa (HSE) (Harada & Sasa, 2005) can be used to calculate the J experimentally, which is suitable in Langevin system in nonequilibrium steady states.

$$J = \Gamma v_s^2 + \Gamma \int_{-\infty}^{\infty} df\left[\tilde{C}(f) - 2T\tilde{R}'(f)\right] \tag{2.1}$$

(Harada & Sasa, 2005, 2006; Toyabe et al., 2010a; Toyabe & Sano, 2008). Here, the v_s is the average rotational velocity. $\tilde{C}(f)$ is the Fourier transform of the self-time correlation function $C(\tau) = \langle[v(t+\tau) - v_s][v(t) - v_s]\rangle$, which represents the rotational velocity fluctuation. $\tilde{R}'(f)$ stands for the real part Fourier transform of the rotational velocity linear-response function, $\langle v(t)\rangle_N = v_s + \int_{-\infty}^{t} ds\, R(t-s)N(s) + O(N^2)$, where $\langle v(t)\rangle_N$ means the ensemble average of $v(t)$ applied with a small enough torque $N(t)$ and the prime represents the real part. $\tilde{R}(f)$ reflects the sensitivity of the rotational velocity to a disturbance at frequency f.

In equilibrium state, the fluctuation-dissipation theorem (FDT) $\tilde{C}(f) = 2T\tilde{R}'(f)$ is valid (Kubo, Toda, & Hashitsume, 2012). However, FDT is broadly violated in nonequlibrium states (Blickle, Speck, Lutz, Seifert, & Bechinger, 2007; Gomez-Solano, Petrosyan, Ciliberto, Chetrite, & Gawędzki, 2009; Mizuno, Tardin, Schmidt, & MacKintosh, 2007; Speck & Seifert, 2006). Eq. (2.1) enables us to calculate the heat dissipation from two parts, the steady motion and nonequilibrium fluctuations, which correspond to the first term and second term in Eq. (2.1), respectively. The method they applied in their experiment can be briefly illustrated as below

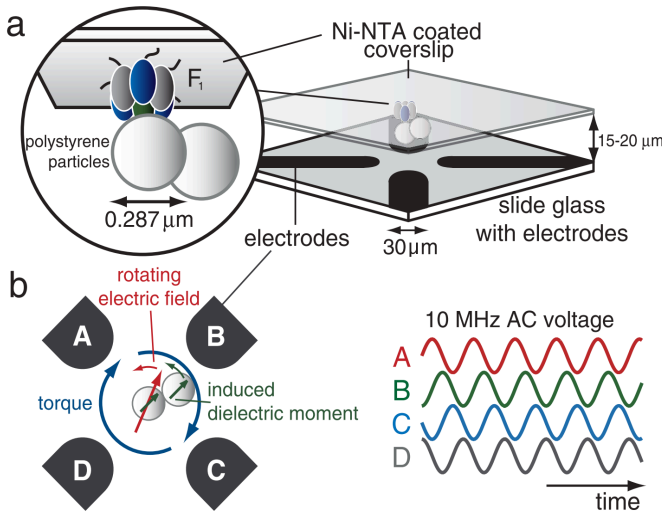

Figure 2-4 Experiment Setup (Toyabe et al., 2010)

The experiment is set up as **a** in Figure 2-4 and constant torque applied and response measurement is using an electrorotation method as shown in **b** of Figure 2-4, where a rotating electric field is generated by four electrodes A, B, C and D, which are applied sinusoidal voltages with a phase shift at the frequency of 10 MHz.

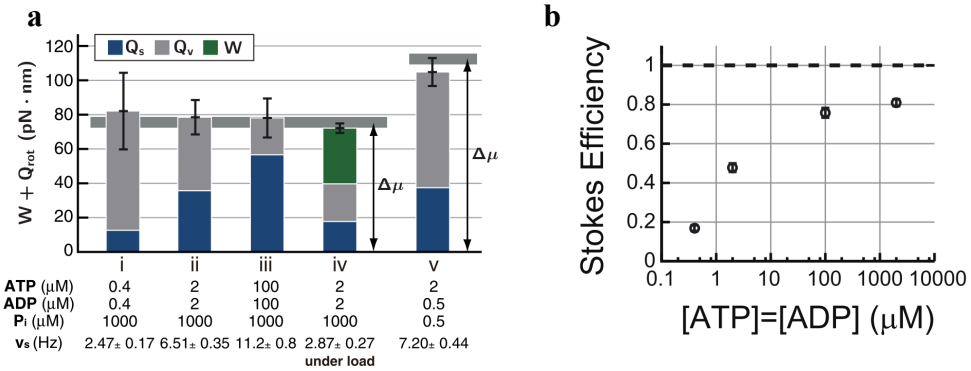

Figure 2-5 Two kinds of dissipation and efficiency (Toyabe et al., 2010)

The results they obtained about work and efficiency can be simply illustrated in Figure 2-5. In **a**, the Q_s(dark blue) means the heat dissipation from steady motion while the Q_v(grey) is the heat dissipation from thermal fluctuation, and the W stands for the work against to the external constant torque. The data under X axis is the concentration of substrates and the mean rotation rate v_s. In addition, the horizontal grey bar is the value of $\Delta\mu$ whose width represents the difference from referenced literatures. The data shows that the sum of heat dissipation from rotation nearly equals to the chemical free energy $\Delta\mu$ within error, in other word, it means the pseudo efficiency $\eta_Q \approx 100\%$. However, the Stokes efficiency η_S defined using the mean rotational speed is far away from 100% and it seems the maximal efficiency is 81% as shown in **b**. Moreover, the Stokes efficiency is dependent on the ATP concentration, which is not observed in other experiments.

2.2.3 Calculating the torque by Fluctuation Theorem

In nonequilibrium statistical mechanics, fluctuation theorem (FT) is a theory used to quantify the entropy production in small nonequilibrium systems and has been applied to colloidal particle systems, granular systems and turbulent system (Ciliberto, Garnier, Hernandez, & Lacpatia, 2004; Feitosa & Menon, 2004; K Hayashi & Takagi, 2007; Kumiko Hayashi, Ueno, Iino, & Noji, 2010; G. M. Wang et al., 2002). Meanwhile, it has also been used to study biological systems (Collin, Ritort, Jarzynski, Smith, & Tinoco, 2005; K Hayashi & Takagi, 2007; Liphardt, Dumont, Smith, & Tinoco, 2002; Mahmud, Campbell, Bishop, & Komarova, 2009; Mizuno et al., 2007). In this experiment (Kumiko Hayashi et al., 2010) , they concentrate on the rotary torque measurement of F_1-ATPase.

They used a Langevin equation to describe the time evolution of the rotation of F_1-ATPase

$$\Gamma\frac{d\theta}{dt} = N + \xi(t), \qquad \langle\xi(t)\xi(t')\rangle = 2\Gamma k_B T\delta(t-t') \tag{2.2}$$

where N is the torque, $\xi(t)$ represents the random force due to the thermal noise, k_B is the Boltzmann constant and T is the room temperature ($T = 25°C$). They assumed N is constant as shown in the previous studies (Noji, Bald, Yasuda, Itoh, & Yoshida, 2001; Sakaki et al., 2005; Yasuda et al., 1998, 2001). Based on above model, the relation between measured quantities and torque is

$$\ln\left[\frac{P(\Delta\theta)}{P(-\Delta\theta)}\right] = N\Delta\theta/k_B T \tag{2.3}$$

here, $\Delta\theta = \theta(t + \Delta t) - \theta(t)$ and $P(\Delta\theta)$ means the probability distribution of $\Delta\theta$ in the 120° rotation. Their results also suggest the work done by constant torque N per step is nearly equivalent to the free energy of an ATP, indicating 100% Stokes efficiency.

2.2.4 Stall torque method

The F_1 motor rotation is affected by the external torque applied (Toyabe et al., 2011). When there is no load, the F_1 motor would rotate in discrete 120° steps at low ATP concentration and go fast and smooth as the ATP concentration increases. If the ATP concentration is fixed and gradually increase the torque applied to the F_1 motor in the opposite direction of ATP synthesis, the F_1 motor would rotate slower and slower as the torque increasing until it demonstrates bidirectional stepwise fluctuation under certain magnitude of torque. This state is called stall state and corresponding torque is named stall torque (N_{stall}). Under the stall torque, the F_1-ATPase reflects $W_{stall} \equiv N_{stall} \times 120°$ work against the external torque in each step. In other words, W_{stall} equals to the maximal work that can be generated by F_1-motor in one step. The results they obtained can be easily understood in the figure below.

They found W_{stall} nearly equals to the free energy of an ATP $\Delta\mu$ in broad range. As shown in Figure 2-6, A: Rotation rates under different ATP(=ADP) concentration. B: Rotations rates under different $\Delta\mu$. C&D: the corresponding maximal work to A and B, respectively.

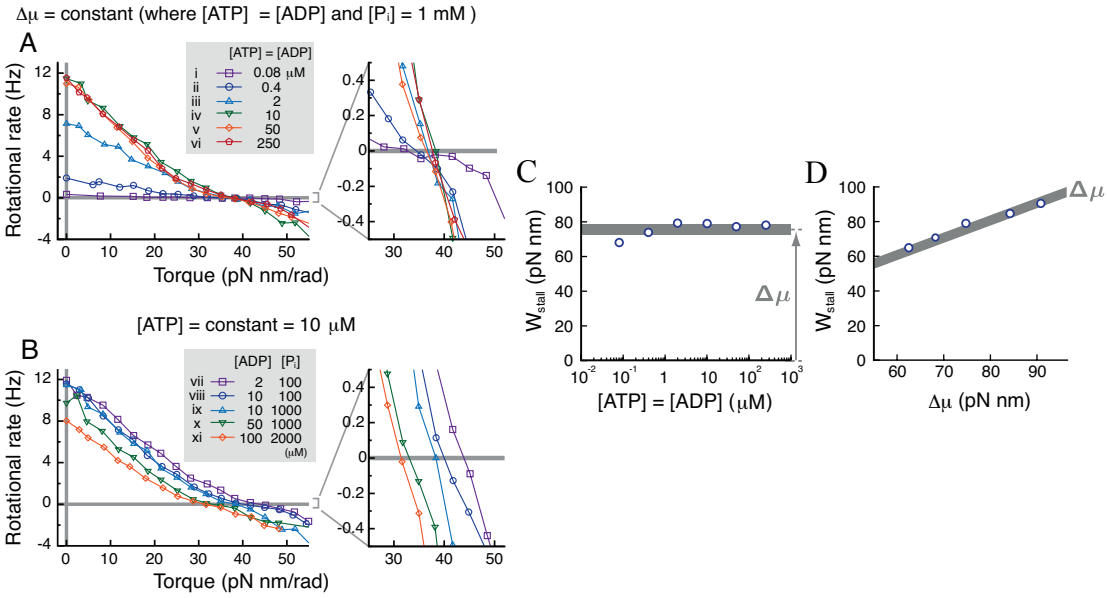

Figure 2-6 Stall torque method (Toyabe et al., 2011)

2.3 Summary

Although experiments introduced above take different methods, their results all prove the pseudo efficiency is nearly 100%, which corresponds step (1) in Figure 2-1. Moreover, the η_Q even exceeds 100% at slow rotation rate range in 2.2.2 and we will investigate the origins by a computational model in the next chapter. In addition, three of them measured the torque generated by F_1 motor directly or indirectly and all of them are quite large in nanometer scales, indicating the 100% Stokes efficiency from the corresponding work. However, the maximal work is based on the condition that the torque is nearly constant during the whole 120° step, which can only be observed from 2.2.1 and is regarded as an assumption in the other experiments. It is worth noting that in 2.2.2 the Stokes efficiency is obviously below 1 , which is quite different with the other experiments, so we will implement the model based on the data of 2.2.2 and try to explain why the pseudo efficiency is nearly 100% and what biological processes can be found to match the behaviours of model from simulation perspective.

3. Stochastic Model and Simulation

3.1 The totally asymmetric allosteric model

To analyze the energy dissipation process quantitatively, Kawaguchi, Sasa and Sagawa (Kyogo Kawaguchi et al., 2014) introduced a simple Markov model with a discrete variable n for the net number of ATP binding/unbinding events and a continuous angular variable x to describe rotary motion. Known as the totally asymmetric allosteric model (TASAM), ATPs binds on the motor randomly with nearly the same probability in any angle of the rotation but only on specific range of angle, products are allowed to be released, which is determined by detailed parameters in the model. In addition, TASAM also incorporates results from previous studies: the discrete steps (Masaike, Koyama-Horibe, & Oiwa, 2008; Yasuda et al., 2001), mechanical potentials (Toyabe et al.,2012) and large stall force (Toyabe et al., 2011).

TASAM model is described in one-dimensional way based on the Brownian motion and potential switching. Because the interaction between γ subunit and $\alpha_3\beta_3$ subunits and the attachment of γ subunit and the probe, the mechanical potentials $U_n(x)$ are created and trap the degree of freedom x of the probe. In addition, for the threefold symmetry of F_1-ATPase, the potentials have translational symmetry every 120°, which means $U_n(x) = U_0(x - 120\times n)$.

There are two sub-steps for a whole 120° rotation described in 1.2, Toyabe et al. made the observation that, ATP hydrolysis reaction in the isolated F_1-motor experiment follows rather quickly after an ATP binding event and proceeds mostly in the forward direction, the two reactions can be combined into an effective single reaction. By further assuming the ATP binding dwell and the hydrolysis dwell potentials are the same harmonic spring constants k the mechanical potential $U_0(x)$ is described in an effective way as shown in Figure 3-1 and derived in Ref. (Toyabe, Ueno, & Muneyuki, 2012).

$$\frac{U_0(x)}{k_BT} = \frac{kx^2}{2} - \log\left[\exp(-klx) + \exp\left(\frac{\widetilde{\Delta\mu}}{k_BT} + \frac{kl^2}{2}\right)\right] \tag{3.1}$$

where $l = 40°, k = 0.0061\text{deg}^{-2}$, $\widetilde{\Delta\mu}$ =5.2 k_BT, which are estimated by previous experiments (D Okuno, Iino, & Noji, 2010; R Watanabe, Okuno, & Sakakihara, 2012; Yasuda et al., 2001) and shown as below:

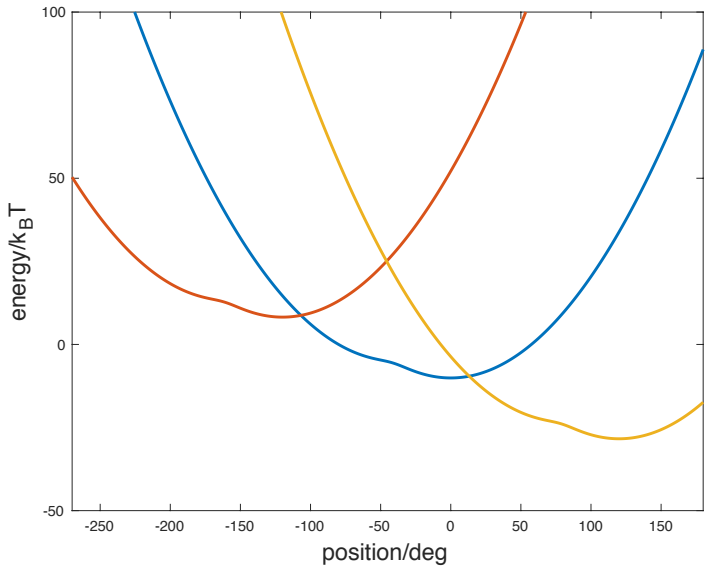

Figure 3-1 The potential $U_n(x)$. where the minimal points for three potentials from left to right are $-120°$, $0°$ and $120°$, respectively.

Due to viscous drag from the surrounding fluid, the position of the probe can be described by an overdamped Langevin equation with potentials:

$$\Gamma\dot{x} = -\frac{\partial}{\partial x}U_n(x) - F + \sqrt{2\Gamma k_BT}\xi(t) \tag{3.2}$$

where Γ is the friction coefficient of the probe, F is the external torque applied on the probe and $\xi(t)$ is the Gaussian white noise with unit variance. Eq. (3.2) is supplemented by a description for potential switching $n \to n \pm 1$ The switching rate in the forward direction $n \to n+1$, $R_n^+(x)$ represents the ATP binding and ADP release reaction and the switching rate in the backward direction $n+1 \to n$, $R_{n+1}^-(x)$ stands for the ADP binding and ATP release. Moreover, they assumed $R_n^{\pm}(x) = R_0^{\pm}(x - 120°\times n)$ in TASAM and only the transition to neighbouring chemical state is allowed. The switching rate function need satisfy the local detailed balance:

$$\frac{R_n^+(x)}{R_{n+1}^-(x)} = \exp\left\{\frac{1}{k_BT}[U_n(x) - U_{n+1}(x) + \Delta\mu]\right\} \tag{3.3}$$

where $\Delta\mu$ is the free energy difference between ATP and ADP + P_i in the solution, and $\Delta\mu$ is calculated by $\Delta\mu = \Delta\mu_0 + k_B T\log([\mathrm{ATP}][\mathrm{H_2O}]/[\mathrm{ADP}][\mathrm{Pi}]), \Delta\mu_0 = 18.3k_B T$. Next, in order to add the effect of the concentration of ATP, they rewrite the $R_n^{\pm}(x)$ and its form is $R_n^{\pm}(x) = W f_n^{\pm}(x)$, where W is related to the concentration of ATP(=ADP) by collision frequency.

To construct a practical potential switching model, they made the following observations. The first one is the chemical reaction need not to happen at an angle, which means the timing of reaction is random with respect to position. Another fact was shown in study (Lebowitz & Spohn, 1999) that there are overlaps between adjacent potential pairs. To reproduce the dissipation-free feature at low rotational velocity regime, they introduced a parameter q to decide the asymmetry of binding and unbinding process to position while satisfying detailed balance as well:

$$\begin{aligned} f_n^{+}(x) &= \exp\left\{\frac{q}{k_B T}[U_n(x) - U_{n+1}(x) + \Delta\mu]\right\} \\ f_{n+1}^{-}(x) &= \exp\left\{\frac{q-1}{k_B T}[U_n(x) - U_{n+1}(x) + \Delta\mu]\right\} \end{aligned} \tag{3.4}$$

Before showing the detailed simulation, we intend to demonstrate more clearly the roles of parameters q and W in TASAM without detailed numerical parameters and introduced two time scales related to TASAM. The parameter q in TASAM is determined by details of the ATP binding process and it can be expressed as below: the ATP would diffuse from the solution to the catalytic sites. However, ATP does not bind successfully once it hits the sites and it may hit the binding site many times before binding to rotate.

W, which stands for the collision frequency or namely switching rate from the right orientation, grows with ATP concentration but not linear in the whole concentration range as shown in next chapter. Besides, q is introduced to determine angular dependence and different value decides different sensitivity of binding on and off as shown in Figure 3-2.

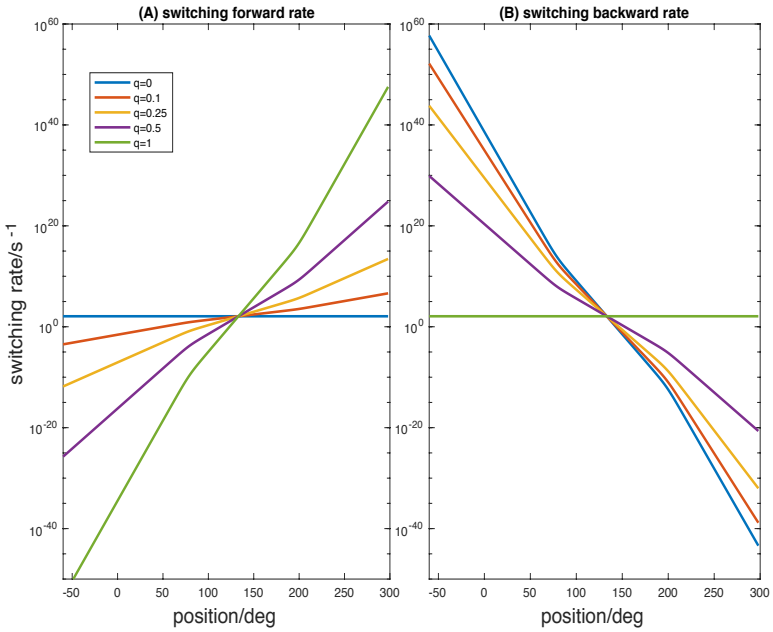

Figure 3-2 Comparison between switching forward rate and switching backward rate based on potential $U_n(x)$ whose minimal point is located in 120° under different q. **A**: the switching forward rate. **B**: the switching backward rate. For example, when $q = 0$, the ATP would bind with constant probability at any degree of a period while at some range, the ATP would kick out immediately but at some range, it would bind on easily. In the opposite, when $q = 1$, the ATP would bind easily at some range but extremely hard at anther range, while it would unbind equally at all the range.

3.2 Langevin simulation

The TASAM as defined by the overdamped Langevin equation (Eq. (3.2)) can be simulated with uniform time stepping.

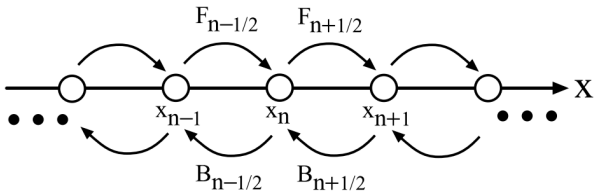

Figure 3-3 Discrete method (WANG et al., 2003)

Their idea is using a spatially discrete Markov chain to produce finite differencing of Eq. (3.2)and the set of discrete sites can be shown in Figure 3-3.

$$\frac{dp_n}{dt} = -\left(B_{n-\frac{1}{2}} + F_{n+\frac{1}{2}}\right)p_n + F_{n-\frac{1}{2}}p_{n-1} + B_{n+\frac{1}{2}}p_{n+1}$$
$$= \left(F_{n-\frac{1}{2}}p_{n-1} - B_{n-\frac{1}{2}}p_n\right) - \left(F_{n+\frac{1}{2}}p_n - B_{n+\frac{1}{2}}p_{n+1}\right) = J_{n-\frac{1}{2}} - J_{n+\frac{1}{2}} \tag{3.5}$$

where, $p_n(t)$ is the probability of finding the γ subunit at site x_n at time t and its form is

$$p_n(t) \approx \int_{x_n-\frac{\Delta x}{2}}^{x_n+\frac{\Delta x}{2}} \rho(x,t)\mathrm{d}x \approx \rho(x_n,t)\Delta x \tag{3.6}$$

because the x_n stands for the interval $(x_n - \frac{1}{2}, x_n + \frac{1}{2})$. $F_{n+\frac{1}{2}}$and $B_{n+\frac{1}{2}}$ are forward and backward transition rate between sites x_n and x_{n+1}, respectively. $J_{n+\frac{1}{2}}$ is the net probability current between x_n and x_{n+1}.

From (WANG, PESKIN, & ELSTON, 2003), the specific forms of $F_{n+\frac{1}{2}}$ and $B_{n+\frac{1}{2}}$ are

$$F_{n+1/2} = \frac{D}{(\Delta x)^2}\frac{\Delta\phi_{n+\frac{1}{2}}/k_BT}{\exp\left(\Delta\phi_{n+\frac{1}{2}}/k_BT\right) - 1} \tag{3.7}$$

$$B_{n+1/2} = \frac{D}{(\Delta x)^2}\frac{-\Delta\phi_{n+\frac{1}{2}}/k_BT}{\exp\left(-\Delta\phi_{n+\frac{1}{2}}/k_BT\right) - 1} \tag{3.8}$$

here, $\Delta\phi_{n+\frac{1}{2}}$ is defined as

$$\Delta\phi_{n+\frac{1}{2}} = \phi(x_{n+1}) - \phi(x_n) \tag{3.9}$$

and here $\phi(x) = U_n(x)$, $D = k_BT/\Gamma$ is the diffusion coefficient.

Next, we use Gillespie's algorithm to simulate trajectories and we calculate cumulative coefficients by above four transition rates.

$$c_k = \frac{1}{c_0}\sum_{j=1}^{k} W_j(\theta,\sigma)\ , c_0 = \sum_{j=1}^{4} W_j(\theta,\sigma) \tag{3.10}$$

Then, simulation is implemented as follows. Firstly, an initial state (θ,σ) is set at time t, then two random numbers, r_1, r_2 which are uniformly distributed in the interval [0,1] are generated. Then, the time interval before next step is given by

$$\Delta t = -\frac{1}{c_0}\ln[r_1] \tag{3.11}$$

Next, the following step is the one chosen by the transition k if $c_{k-1} < r_2 < c_k$. The system is updated as following:

$$t \to t + \Delta t$$
$$(\theta, \sigma) \to (\theta', \sigma') \tag{3.12}$$

All the operations are repeated until the final time. Three samples of trajectories are shown bellow

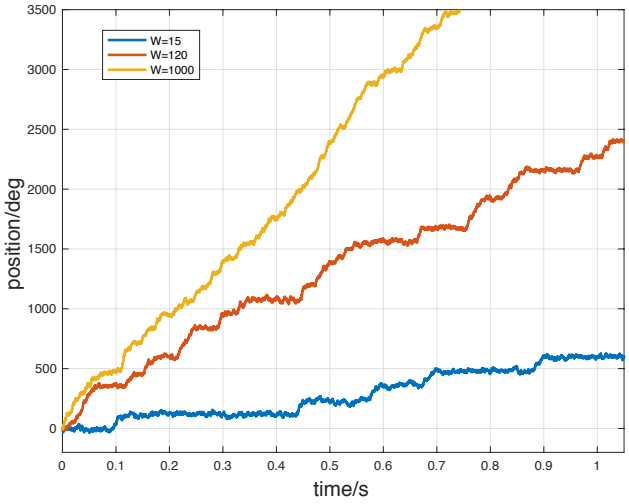

Figure 3-4 Sample Trajectories of F_1 Motor. $D = 47520, dx = 2, FL = 0, k_BT = 4.1, q = 0, W = 15, \Delta\mu = 18.3k_BT$. the mean time interval generated automatically by Gillespie's algorithm is 4.2×10^{-5}s.

Above three trajectories are with different W and correspond to different behaviors of different ATP concentration. When W is small, the γ subunit would show obvious step-wise path and the ATP waiting time between switches is relatively long (blue line). Demonstrated as the red line, when W increase, the step-wise path still exists while the waiting time becomes short, so the mean rotational velocity increases as well. When W becomes big further, we nearly cannot observe the waiting process in the trajectory, so the step-wise behavior vanishes as the W increasing.

Although Langevin simulation is easy to implement, it is computational expensive to obtain accurate average quantities such as rotational velocity, steady-state distribution and heat flow between system and environment (HFSE). Actually, what we focus is the properties reflected by the ensemble average of TASAM instead of any single trajectory, so we use Fokker-Planck equation to describe this model that is mathematical equivalent to the Langevin equation in terms of the ensemble behaviors (Sekimoto, 2010), which use probability density function to characterize the positions and states of a particle. Although the study (Kyogo Kawaguchi et al., 2014) has stated they use Fokker-Planck simulation to solve their model, they did not give the explicit process of simulation, and from the processes we implemented, it is full of considerations and details, so we next demonstrated the details of Fokker-Planck simulation of TASAM.

3.3 Fokker-Planck equation and simulation

3.3.1 The Fokker-Planck equation for F_1-motor

The TASAM introduced by Kawaguchi et al leads to the following Fokker-Planck euqation for the set of distribution functions $\rho_n(x,t)$ of the rotational angular variable x at time t, where $n = \pm1, \pm2, \ldots$ is the net number of ATP binding events,

$$\begin{aligned}&\frac{\partial \rho_n}{\partial t} = D\frac{\partial}{\partial x}\left(\frac{1}{k_B T}\frac{\partial U_n(x)}{\partial x}\rho_n + \frac{\partial}{\partial x}\rho_n\right)\\&+R^+_{n-1}(x)\rho_{n-1} + R^-_{n+1}(x)\rho_{n+1} - \left(R^+_n(x) + R^-_n(x)\right)\rho_n\end{aligned} \tag{3.13}$$

here

$$R^+_n(x) = W\exp\left\{\frac{q}{k_B T}[U_n(x) - U_{n+1}(x) + \Delta\mu]\right\}$$

$$R^-_n(x) = W\exp\left\{\frac{q-1}{k_B T}[U_n(x) - U_{n+1}(x) + \Delta\mu]\right\}$$

and $U_n(x) = U_0(x - n\times120°)$

It is not feasible to solve the infinite set of coupled PDEs numerically. Below we introduce a physics-based approximation which is expected to become increasingly accurate as the steady-state is approached.

3.3.2 Equation governing the steady-state distribution

To motivate approximation, we use Langevin simulation and make an ansatz to investigate the property of the solution of above equation set, checking how n changes with t.

Starting from an initial value, say $n = 0$, the number of net ATP binding events is well described by a biased random walk at long times. The distribution of n is thus centered around a mean value proportional to t and has a width that increase as $t^{1/2}$. To be definite, we consider an initial state where $x = 0°$ and $n = 0$ at $t = 0$. We collected 9 trajectories from the Langevin simulation. Figure 3-5 shows the statistics of x values at $n = 1,2, \ldots 6$ up to $t \to \infty$. The distribution at much larger n values are shown in Figure 3-6. It is seen from the plots sets, apart from some statistical uncertainties, the distribution at different n approach the same shape apart from a 'shift $n\times120°$'.

For n in the middle of this distribution, $\rho_n(x,t)$ is expected to reach a 'steady-state' distribution $P_n^{ss}(x - n\times120°)$ independent of t. When n is far away from the initial value, which means the n undoubtful has reach the steady state, the distributions are similar to the distribution solved by Fokker-Planck simulation, which has a main peak on 120° with a small peak on around 60° as shown in Figure 3-6.

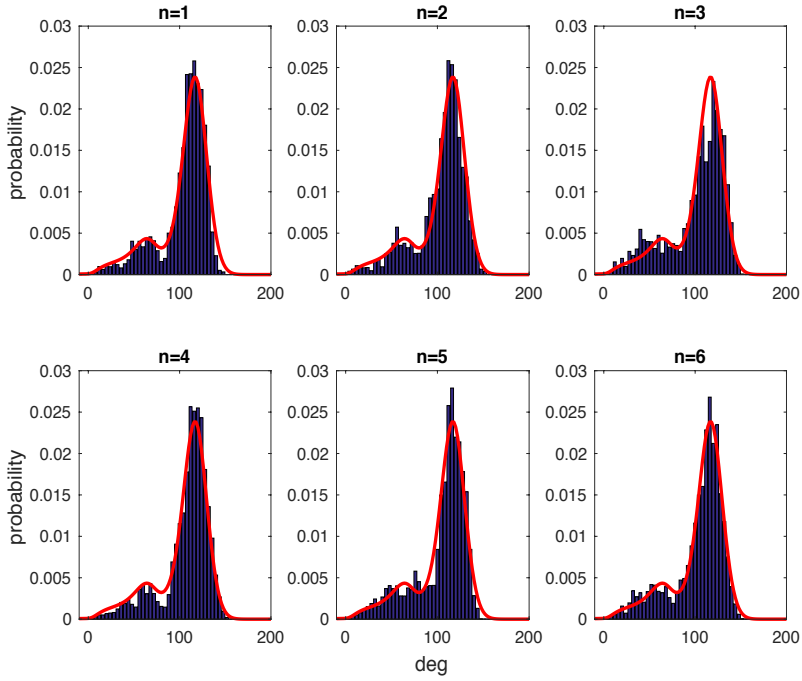

Figure 3-5 The probability distributions under different potential n. $dx = 4, W = 120, q = 0$. Each distribution is averaged by 9 trajectories.

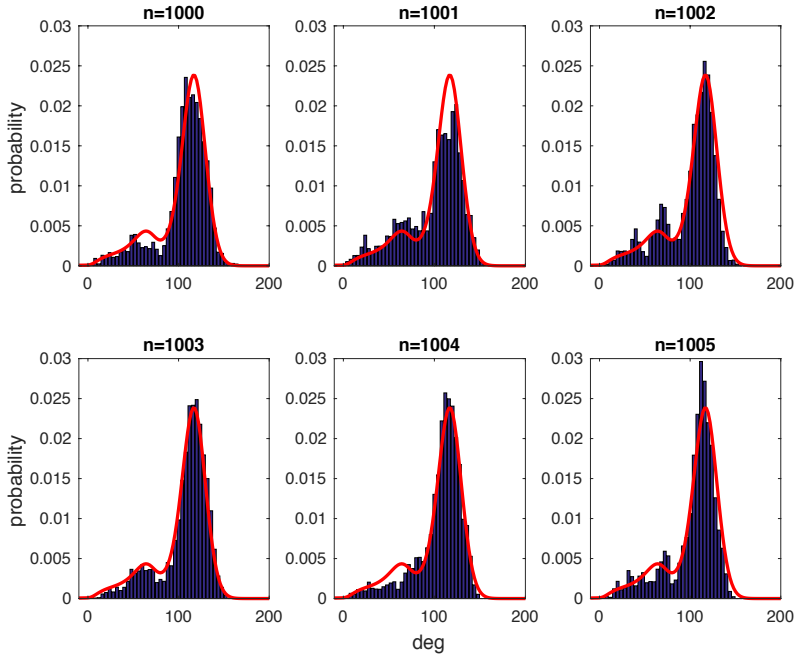

Figure 3-6 The distributions of different n far away from the initial condition. $dx = 4, W = 120, q = 0$. Each distribution is averaged by 9 trajectories.

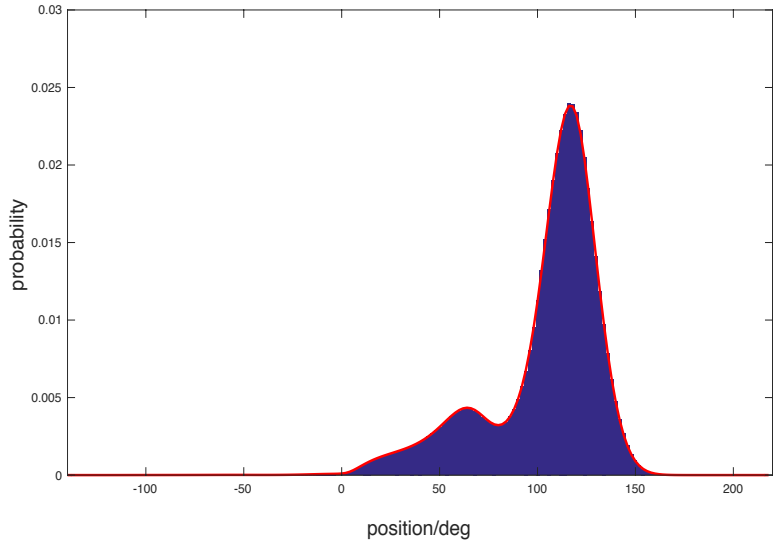

Figure 3-7 The comparison between the averaged result from Langevin simulation and Fokker-Planck simulation with the same parameters.

The key observation is that, in a given realization of the stochastic process, the integer variable n that describes the net number of ATP binding events in a time t follows a random-walk like biased diffusion. When we average over the ensemble, the distribution of $n(t)$, $P\ (n,t)$, approaches that of a Gaussian with a width that increases as $t^{1/2}$. The functions $\rho_n(x,t)$ for n close to its mean value at time t, on the other hand, are expected to become similar to each other in shape after shifting by an amount $n\times120°$ in accordance with $U_n(x)$. This motivates the factorization approximation,

$$\rho_n(x,t) = P(n,t)\rho(x - n\times120°\,,t) \tag{3.14}$$

from the normalization condition

$$\sum_n \int_{-\infty}^{\infty} \rho_n(x,t)dx = 1$$

we require separately

$$\sum_n P(n,t) = 1 \text{ and } \int_{-\infty}^{\infty} \rho_n(x,t)dx = 1$$

Substituting Eq. (3.14) into Eq. (3.13), we obtain the following equation for $P\ (n,t)\ \rho\ (y,t)$ where the dependence on n is absorbed into the variable $y = x - n\times120°$

$$\begin{aligned}
&\frac{\partial P(n,t)\rho(y,t)}{\partial t} = D\frac{\partial}{\partial y}\left(\frac{1}{k_BT}\frac{\partial U_0(y)}{\partial y}P(n,t)\rho(y,t) + \frac{\partial}{\partial y}P(n,t)\rho(y,t)\right)\\
&+R_0^+(y+120°)P(n-1,t)\rho(y+120°,n)\\
&+R_0^-(y-120°)P(n+1,t)\rho(y-120°,t)\\
&-\big(R_0^+(y)+R_0^-(y)\big)P(n,t)\rho(y,t)
\end{aligned}$$

and making use of the fact that $P(n,t)$ is a slow varying function of n at long times, which means $P(n,t) = P(n-1,t) = P\ (n+1,t)$ when $t\to\infty$, we obtain the following equation for $\rho\ (y,t)$

$$\begin{aligned}
&\frac{\partial \rho(y,t)}{\partial t} = D\frac{\partial}{\partial y}\left(\frac{1}{k_BT}\frac{\partial U_0(y)}{\partial y}\rho(y,t) + \frac{\partial}{\partial y}\rho(y,t)\right)\\
&+R_0^+(y+120°)\rho(y+120°,n) + R_0^-(y-120°)\rho(y-120°,t)\\
&-(R_0^+(y)+R_0^-(y))\rho(y,t)
\end{aligned} \tag{3.15}$$

For the equation that contains remaining terms that depend on n explicitly, we integrate over x to obtain,

$$\frac{\partial P(n,t)}{\partial t} = \tilde{R}_0^+\big(P(n-1,t) - P(n,t)\big) + \tilde{R}_0^-\big(P(n+1,t) - P(n,t)\big) \tag{3.16}$$

here

$$\tilde{R}_0^+ = \int_{-\infty}^{\infty} dy R_0^+(y)\rho(y,t)\,,\tilde{R}_0^- = \int_{-\infty}^{\infty} dy R_0^-(y)\rho(y,t)$$

are the total binding (forward) and unbinding (backward) rates, respectively. In general, the two rates are not equal, so Eq.(3.16) describes a biased diffusion process.

Eq. (3.15) can now be solved using numerical methods introduced below.

3.4 Difference scheme

When it comes to numerical simulation, we have to choose appropriate Δx and Δt to keep the simulation stable according to different parameters. However, because what we focus is the results of model simulation instead of the simulation itself, we just take the Crank–Nicolson discretization in time to Eq. (3.13) but do not refer too much mathematics.

Study (WANG et al., 2003) has shown the numerical method is second-order accurate and has a second-order local truncation error in both time and space, meanwhile it is stable. In addition, they use Lax equivalence theorem to prove it converges and global error is second order both in time and space.

Then we just demonstrate the difference scheme of Eq. (3.15) by Crank–Nicolson method.

$$\begin{aligned}\frac{P_j^{n+1}-P_j^n}{\Delta t} &= -\left(B_{n-\frac{1}{2}}+F_{n+\frac{1}{2}}+k_{21}+k_{23}\right)\frac{P_j^{n+1}+P_j^n}{2}\\ &+F_{n-\frac{1}{2}}\frac{P_{j-1}^{n+1}+P_{j-1}^n}{2}+B_{n+\frac{1}{2}}\frac{P_{j+1}^{n+1}+P_{j+1}^n}{2}+(R_1^+\mathbb{L}+R_3^-\mathbb{R})\frac{P_j^{n+1}+P_j^n}{2}\end{aligned} \tag{3.17}$$

where P_j^n is the probability density to find γ subunit in lattice j at time n, $B_{n-\frac{1}{2}}$ and $F_{n+\frac{1}{2}}$ are moving transition rates corresponding to Eq. (3.7)-(3.8), $R_n^{\pm}$ is the switching transition rate from state i to j corresponding to Eq. (3.3)-(3.4) and $\mathbb{L}$, $\mathbb{R}$ are translation operates with 120° to left and right, respectively. Then, we can construct Matrix according to Eq. (3.17) and updates by Eq.(3.18)

$$M_{n+1}P_j^{n+1}=M_nP_j^n\ ,j=1,2,\cdots L,n=1,2,\cdots T \tag{3.18}$$

here, T and L are the lengths of time and space discretization.

Since we have to get the ensemble averaged quantities of TASAM in steady state, most results of simulation are obtained by Fokker-Planck simulation while in some cases, we just use Langevin simulation to check the results when the steady-state distribution solved by Fokker-Planck equation is not very concentrated. In our numerical window, we could get the probability density function in steady state, $P_n^{ss}(x)$, from which we could obtain all the quantities we are interested in.

3.5 The physical quantities

The same as the $U_n(x)$, the $P_n^{ss}(x) = P_0^{ss}(x - 120{\times}n)$ because of the translational symmetry. Next, TASAM further define the $\Lambda_n^{ss}(x) \coloneqq P_n^{ss}(x)R_n^+(x) - P_{n+1}^{ss}(x)R_{n+1}^-(x)$ to characterize the switching position. The first term and second term on the right-hand side stand for the probability density of the position at which the forward switching and backward switching occur, respectively. From this definition, we can obtain the steady-state rotary rotational velocity by $v \coloneqq \int_{-\infty}^{\infty} dx\Lambda_n(x)/3$. Furthermore, as the definition of HFSE in their model, the steady-state average heat dissipation every 120° step, which is calculated as following:

$$Q_{int} \coloneqq \frac{1}{3v}\int dx\Lambda_n(x)[U_n(x) - U_{n+1}(x) + \Delta\mu] \tag{3.19}$$

$$Q_{ext} \coloneqq |\Delta\mu - FL| - Q_{int} \tag{3.20}$$

here FL is the work applied by external torque per forward step, and above two definitions are also consistent with the rate of energy dissipation in the standard formula (Lebowitz & Spohn, 1999; H. Qian, 2007; Seifert, 2005).

$$\dot{W} = \frac{1}{2\beta}\sum_{X,X'} J(X|X')ln\frac{\omega(X|X')}{\omega(X'|X)} \tag{3.21}$$

where $\beta = 1/k_BT$, $\omega(X|X')$ is the transition rate from state X' to X, $J(X|X') = \omega(X|X')P(X') - \omega(X'|X)P(X)$ is the net flux from X' to X, and $P(X)$ is the probability for state X. Next, I would prove Eq. (3.19) and (3.21) are equivalent.

From quantities defined in TASAM, the time for F_1-ATPase rotates one step is $t_s = \frac{1}{3v}$, so the dissipation rate of TASAM is $\dot{W} = \frac{Q_{int}}{t_s} = \frac{3v}{1}\times\frac{1}{3v}\int dx\Lambda_n(x)[U_n(x) - U_{n+1}(x) + \Delta\mu] = \int dx\Lambda_n(x)[U_n(x) - U_{n+1}(x) + \Delta\mu] = \frac{1}{\beta}\times\sum(P_n^{ss}(x)R_n^+(x) - P_{n+1}^{ss}(x)R_{n+1}^-(x))\times\ln(\exp(\beta[U_n(x) - U_{n+1}(x) + \Delta\mu]))$.

In TASAM, $P_n^{ss}(x)$ has the same meaning of $J(X|X')$ and $\ln(\frac{R_n^+(x)}{R_{n+1}^-(x)})$ is equivalent to $\ln(\exp(\beta[U_n(x) - U_{n+1}(x) + \Delta\mu]))$. In addition, because the states are pairs which means we only need count once for a pair of state, so there is no $1/2$ as shown at the head of right side head of Eq. (3.19). Therefore, I have valid Eq. (3.19)satisfy the form of Eq. (3.21).

3.6 Simulation performance

In addition, we need to reference the convergence of simulated quantities we are interested in. The direct result of our simulation is steady-state distribution. However, there is not analytical solution to compare and we cannot distinguish the performance of simulation under different Δt. So, we compare the relation between Δt and mean rotational velocity on $W = 120, q = 0$. In our comparison, there are three quantities are involved, Δt, mean rotational velocity V_s and the runtimes corresponding.

As we can see in Figure 3-8, the mean rotational velocity converges from right to left and the runtime rises from right to left. Take the convergence of mean rotational velocity and the runtime into consideration, we think the value, $\Delta t = 5\times10^{-7}$, is the best choice.

In conclude, we choose $\Delta t = 5\times10^{-7}$ as the time interval when $W < 1000$ and we still need to adjust according to the specific circumstance.

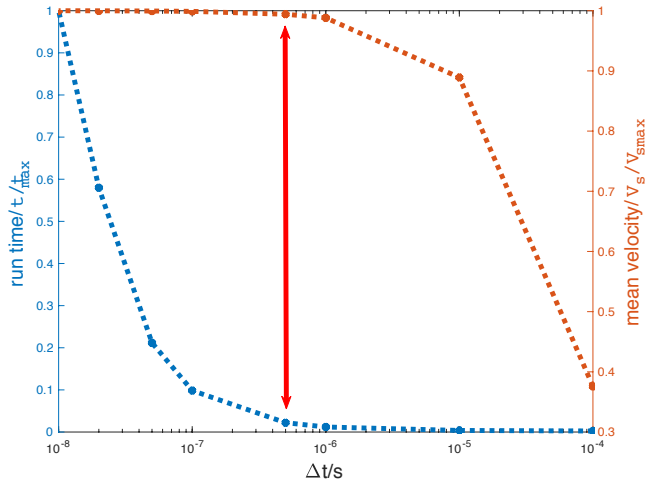

Figure 3-8 The simulation performance based on mean rotational velocity convergence and runtime we used. The orange dash line means the mean rotational velocity change with Δt and the blue dash line represents the runtime change with Δt. Both dash lines are normalized by their maximal value we obtained. We want the mean rotational velocity approach the convergent value but the runtime is not too long, which can be measured by the distance between dot pairs between two dash lines. The double arrows line points out the biggest distance dot pairs among all, which is estimated by eyes. $V_{smax} = 7.13$ Hz, $\text{runtime}_{max} = 78.39\ s$

4. Numerical results and analysis

Having implemented methods in the previous chapter, we would show detailed numerical results here. At first, we demonstrate the change of steady-state distribution under potential centered on 120° with different q and W as shown in Figure 4-1 and Figure 4-2, respectively.

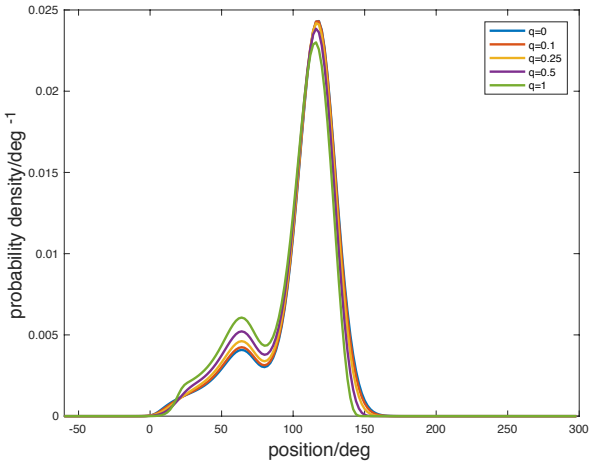

Figure 4-1 The steady-state distribution under different q, $W = 105$.

As shown in Figure 4-1, under the same $W = 105$, the steady distributions demonstrate a bit difference under different q. The most noticeable difference is the height of peaks on around 80° and on the 120°. Actually, the small peak is caused by a simple reason. If we carefully observe the shape of the potential as shown in Figure 3-1, we could find a flat on around 60°, which stands for the intersection of 80-degree sub-step and 40-degree sub-step. Therefore, the probability flow would accumulate around that point. As the W increasing, the flow moves fast and the flow leaving 60° point leaves much faster and so does the flow coming to 60°. So, we could find the small peak grow higher when W increase.

From $q = 0$ to 1, the height of peak on 120° decrease while the height of peak on around 60° increases. In addition, the width of the whole distribution noticeable becomes narrow slightly from $q = 0$ to 1.

As demonstrated in Figure 4-2, the steady-state distribution changes relatively large with the W increasing. Actually, there are 12 lines and corresponding W is from 0.0001×2^{0} to 0.0001×2^{23} by every 2^{2} in geometric progression. When W approaches zero, the steady-state distributions approach equilibrium distribution, which correspond the distributions with relatively high peak under 120° and without obvious peak under around 60°. However, as W increasing, the peak under 120° decreases fast and the peak under about 60° increase fast.

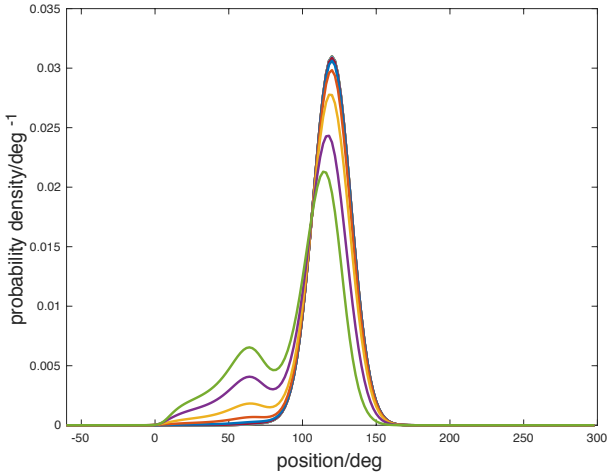

Figure 4-2 The steady-state distribution under different W, $q = 0$.

Literally speaking, we are more interested in the net switching rate density, $\Lambda_n^{ss}(x)$, because it directly relates to all the physical quantities we want. Next, we would show how we obtain the $\Lambda_n^{ss}(x)$.

As shown in **a** of Figure 4-3, the $\Lambda_n^{ss}(x)$ is calculated by $P_n^{ss}(x)R_n^{+}(x) - P_{n+1}^{ss}(x)R_{n+1}^{-}(x)$. Since we set the condition that hydrolysis reaction of the F_1-motor is the positive reaction, it is reasonable that the switching probability density rate of switching forward flow (blue line) is more than the backward flow (red line), in this way can the γ subunit of this model move forward. And from Figure 4-3, we also can tell that ATPs would bind on in relatively large angular range while for most range, they are just kicked out totally. Only in a small range, the probability of binding on is large than the probability of unbinding, resulting the behaviour of angular dependence of ATP binding successfully. It is worth noting that the $\Lambda_n^{ss}(x)$ is contributed mainly by the steady-state distribution on the right shoulder of the higher peak.

We call, in our numerical window, the potential centred on $0°, 120°$ and $240°$, potential 1, potential 2 and potential 3, respectively.

We are back to the numerical results under different parameters. The steady-state distributions do not change obviously, but the net switching rate density $\Lambda_n^{ss}(x)$ varies dramatically with different parameter q and W.

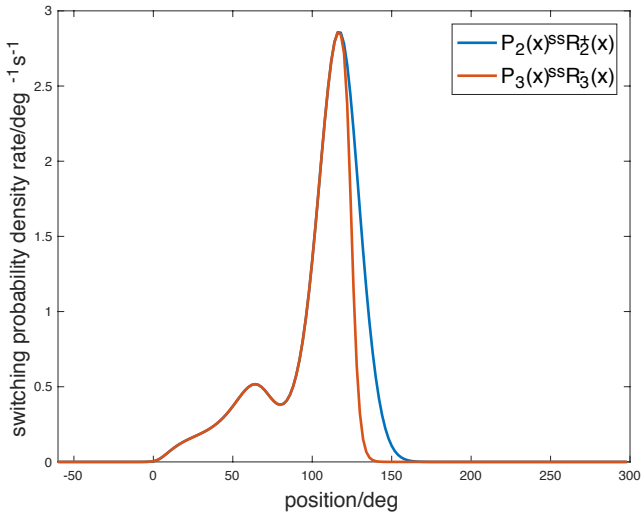

Figure 4-3 The $\Lambda_n^{ss}(x)$. The switching probability density rate of switching forward flow (blue line) and backward flow (red line) from potential 2 to potential 3, and the difference between these two lines is the net switching probability density rate of forward switching. $W = 120$, $q = 0$.

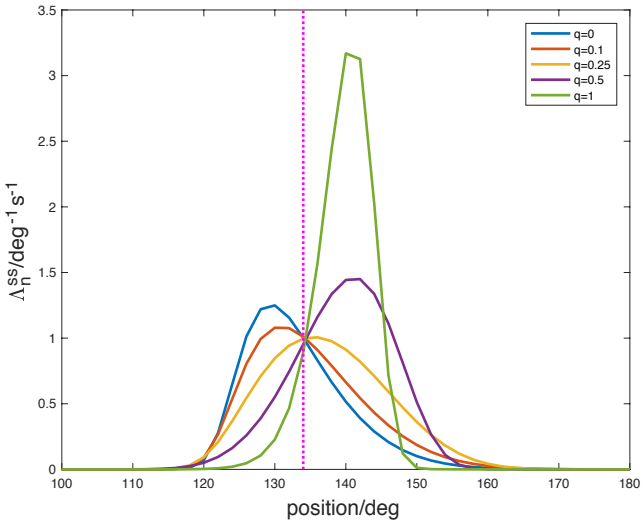

Figure 4-4 $\Lambda_n^{ss}(x)$ under different q. Here, the dash line is the intersection point between potential 2 and potential 3.

Figure 4-4 is corresponding $\Lambda_n^{ss}(x)$ of Figure 4-1 and the difference is very large compared to steady-state distribution. Firstly, the peak moves non-linearly from left-hand side to right-hand side of intersection point as q raises from 0 to 1. Secondly, the area of each distribution varies largely among different q, resulting in largely rotational velocity difference which will be demonstrated later.

The same as the trend under different q, the $\Lambda_n^{ss}(x)$ under different W also change largely. In Figure 4-5, which corresponds to the steady-state in Figure 4-2. There are also 12 distributions, however, we can just distinguish about 5 of them because other 7 ones are very small comparing to the obvious 5 ones. It is also what the rotational velocity difference comes from.

4.1 The rotational velocity as a function of parameter q and W

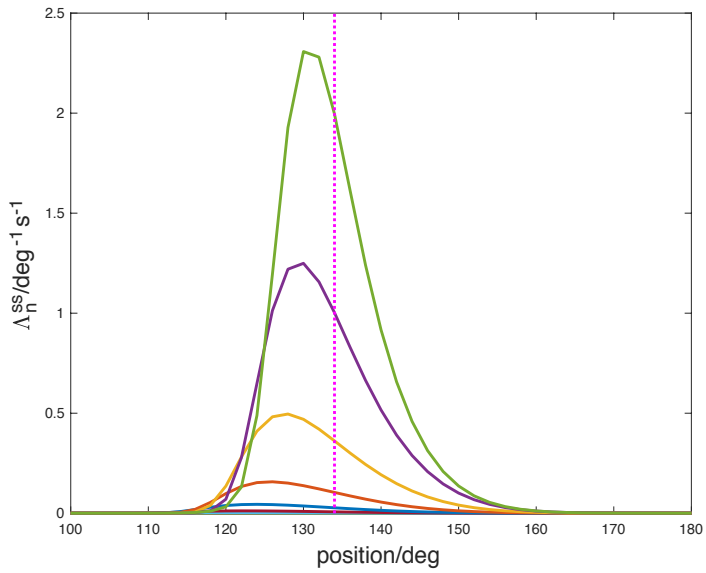

Figure 4-5 The $\Lambda_n^{ss}(x)$ under different W. There are 12 curves in this figure. The higher the peak is the bigger the W is, W is from 0.0001×2^0 to 0.0001×2^{30} by every 2^2 in geometric progression. As the W increases, the peaks approach the intersection point (dash line). $q = 0$. The dash line means the intersection point between potential 2 and

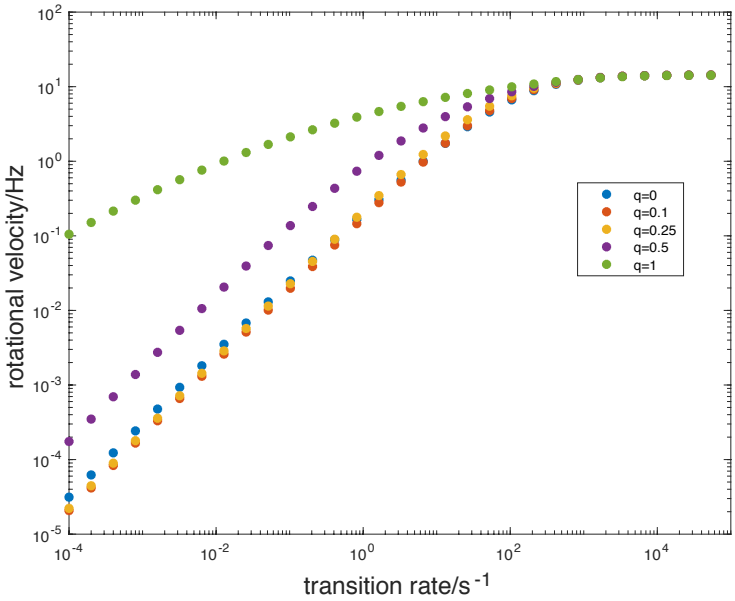

Figure 4-6 The rotational rotational velocity change under q and W. W is from 0.0001×2^0 to 0.0001×2^{29} by 2 in geometric progression.

Then, we would show the rotational velocity change affected by these two parameters demonstrated in Figure 4-6. At small W range and for different q, the rotational velocity nearly equals to each other except rotational velocity with $q = 1$ is much larger than others. For all q, the rotational velocity would increase as the W increasing until it approaching a maximal rotational velocity. In addition, All the rotational velocity curves would approach the same maximal rotational velocity as W approach infinite large.

4.2 Time scales

Then, we should notice there are two key time scales in TASAM. For simplicity, we just treat $U_0(x)$ as a harmonic potential and k in $U_0(x)$ as the spring constant and corresponding time scales are estimated based on this simplification. The first one is $\tau_v = \Gamma L^2/(kL)^2$, which determines the rotational velocity saturation. Another one is $\tau_p = \Gamma/k$, which represents the time scale of relaxation time in a single potential and the values of them based on TASAM are $\tau_v = 3.9\times10^{-5}s$ and $\tau_p = 3.4\times10^{-3}s$, respectively as demonstrated in Figure 4-7.

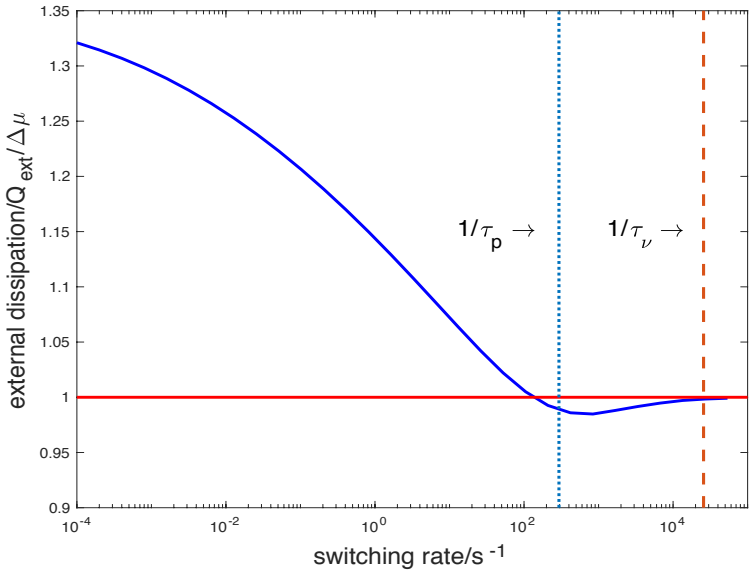

Figure 4-7 Two key time scales and the switching rate-external dissipation diagram. The external dissipation is divided by $\Delta\mu$. The blue curve is the external dissipation change with switching rate. The red line is the referenced line for 100% external dissipation. The curve would drop from the very beginning until around $1/\tau_p$ and become close to $\Delta\mu$ as approaching $1/\tau_v$.

4.3 Heat dissipation

Next, we would show the heat dissipation relation with all the parameters and we produced the rotational velocity-external dissipation relation in TASAM. We just set W from 0.0001×2^0 to 0.0001×2^{39} by 2 in geometric progression and obtain the rotational velocity and external dissipation according to Eq. (3.19) and Eq. (3.20) at different q. Although we have applied all the parameters as the study (K Kawaguchi, Sasa, & Sagawa, 2014) suggested, we can only obtained the rotational velocity-external dissipation diagram with similar behaviors but not exactly the same as the origin as shown in **a** of Figure 4-9.

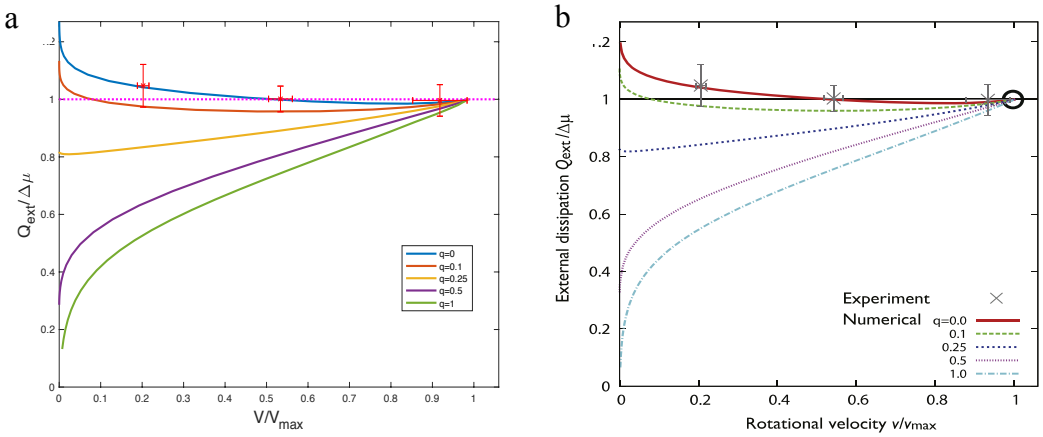

Figure 4-9 Comparison of simulation results and figure from model paper (K Kawaguchi et al., 2014). **a**: our simulation result. **b**: the result from model paper. The X axis represents the rotational velocity, Y axis means the external dissipation and they are normalized by V_{max} and $\Delta\mu$, respectively.

In fact, the biggest difference of them is the maximal rotational velocity, which is around 14.5 Hz in **a** and 12 Hz in **b**, respectively in Figure 4-9. No matter which q we choose, we observed that curves would approach the same point as $W \to \infty$, which is maximal rotational velocity this model could reach. In order to understand the difference, we try multiplying the rotational velocity of our results with 81% according to the Stokes efficiency demonstrated in 2.2.2. Finally, we obtain nearly the same curves as the original model except for some details may due to the numerical method.

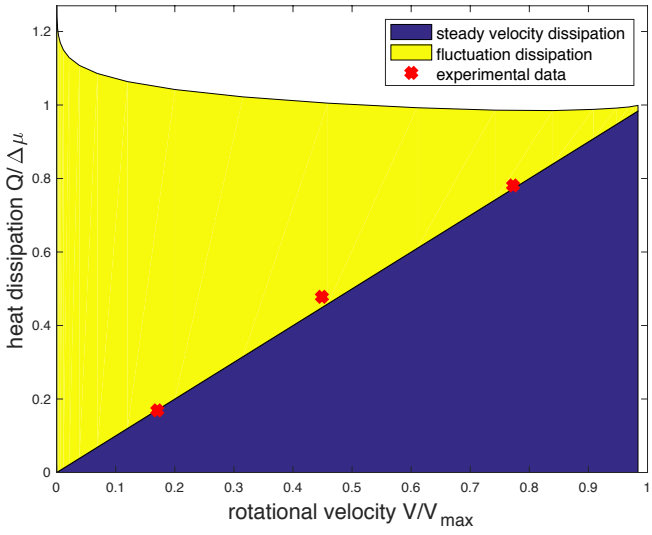

Figure 4-8 The different dissipation calculated from TASAM. The cyan dots represent experimental data. $q = 0, \Gamma = 15.52\ p\text{N nm/Hz}$

Furthermore, in order to compare the performance of TASAM to reproduce the dissipation from steady-rotational velocity rotational velocity and fluctuation, we obtained Figure 4-8.

The blue portion is the dissipation from steady rotational velocity, the yellow portion is the dissipation from fluctuation and the red crosses are experimental data. Since the X axis represents the rotational velocity and the steady rotational velocity dissipation is calculated by Stokes' Law that $Q_s = \Gamma V_s^2 / (3V_s)$, where Γ is the friction coefficient and V_s means the mean rotational velocity, the Stokes' efficiency is proportional to the mean rotational velocity. Plus, we also can observe from above figure that the Stokes efficiency obtained by experiment is well reproduced by TASAM. We need point out that the above figure is based on our simulation, which the maximal rotational velocity is around 14.5Hz. However, there is no obvious difference when we multiplying rotational velocity we obtained with 81% and set the maximal rotational velocity as 12Hz as mentioned above.

Although the method that multiplying 81% is by artificial and there are inconsistences in Stokes efficiency between experiment 2.2.2 with other experiments, this model reflects well agreement of process that converting the chemical energy to mechanical energy of γ subunit that is shown as (1) step in Figure 2-1. Therefore, we plan to investigate the dynamics with high energy conversation efficiency reflected by this model, relate them with observed biological process and try to explain the disagreements between TASAM and other observations.

5. Energy conversion efficiency

5.1 Energy conversion efficiency analysis of wild type

Actually, with different values of q, the TASAM is so flexible to generate different amount HFSE comparing to $\Delta\mu$ as shown in Figure 4-9, so it no wonder that results are consistent with the experiments with specific q. However, the angular dependence parameter q may have essential meaning not only in TASAM but also correspond real behaviors of F_1-motor and we can go further by studying its dynamics. So, at first, we would demonstrate the roles of parameter q in simulation and other features of the TASAM in the aspect of energy conversion. Since this model and experiments are based on the data from wild type of F_1-ATPase, the properties belong to wild type.

As shown in Figure 4-4, the peak of Λ_n^{ss}(x) moves from left-hand side to the right-hand side of the intersection point between potentials, importantly, where does the switch happen affects the value of HFSE, which can be positive or negative (Figure 5-1) according to TASAM. The parameter q plays a crucial role in the net probability density rate of forward switching because it can control the distribution of net flow which is demonstrated in Figure 4-4, in other word, it can decide the value of HFSE.

In addition, q also can affect the amount of switching forward flow by manipulating the dependence of $U_n(x) - U_{n+1}(x) + \Delta\mu$ according to Eq. (3.4). So, in TASAM, q influences both the efficiency and rotational velocity under the same W as also shown in Figure 4-4.

W, the switching rate, has obvious effect on the amount of switching forward flow based on $R_n^{\pm}(x) = W f_n^{\pm}(x)$. Besides, with the switching dynamic, the peak of $\Lambda_n^{ss}(x)$ under different q approaches the intersection point as W increases (Figure 5-2), so no matter what the pseudo efficiencies are at the low W, the pseudo efficiencies would approaches 100% and be independent of the form of Eq. (3.4) as W approaches infinity (Kyogo Kawaguchi et al., 2014).

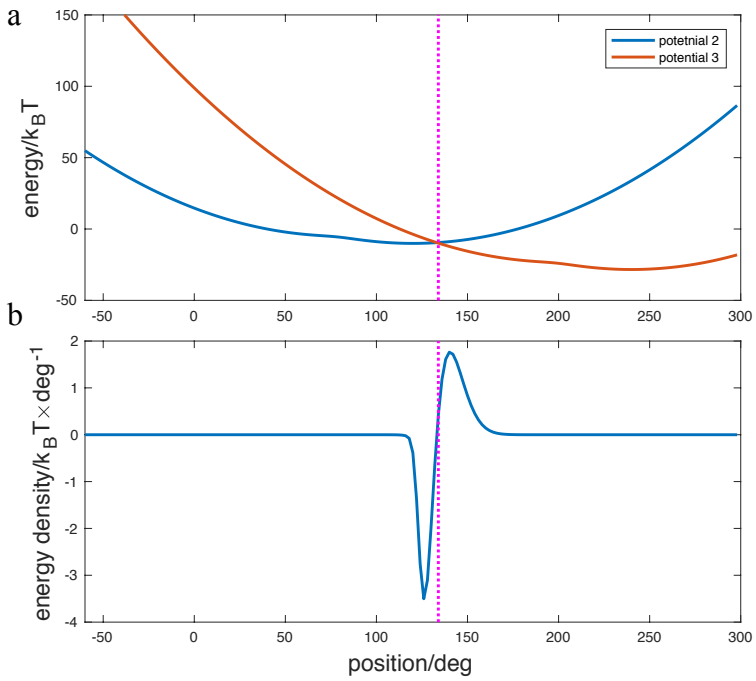

Figure 5-1 The calculation of HFSE. **a**: the chemical potentials. **b**: the net switching probability density rate times the energy difference of two adjacent potentials in **a**. The sum of the vector area represents the HFSE due to the switching (-0.1647pN nm). $W = 120, q = 0$ and the dash line means the intersection point.

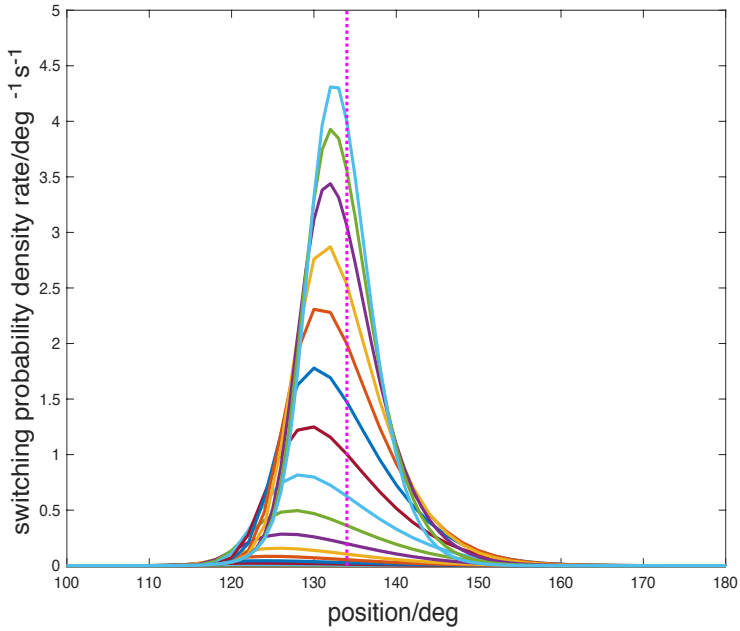

Figure 5-2 The relation between W and the peak of $\Lambda_n^{ss}(x)$. The higher the peak is the big the W is. As the W increases, the peaks approach the intersection point (dash line), $q = 0$.

The simulation results of TASAM suggest that two essential facts are important for the high efficiency of the motor, 1) the negative HFSE in slow rotational velocity range and 2) majority of switching events taking place around the intersection point between potentials at successive n values. The conditions for them to happen will be discussed later. They are fulfilled in the wild type motor, which has been evolved for a long time. To answer the question why they can perform so well in energy conversion, we can disturb its structure and see what happens. On the one hand, we can conduct it in experiments by generating mutants, on the other hand, we can investigate it in simulation if the referenced model (Kyogo Kawaguchi et al., 2014) is good enough to capture the main characteristics. Based on this idea, we did following work under the assumption that the shape of the potential would change in some mutants and $\Delta\mu$ would be change in board range while the dynamics of the F_1-motor still follows TASAM.

5.2 Efficiency change corresponding to potential height

In another study (George Oster & Wang, 2000), it was suggested that the motor generates a constant torque contributes a lot to the high efficiency and it also suggests the Stokes efficiency would approach 100% if the potential between switching points is a constant slope (Hongyun Wang & Oster, 2002). Unfortunately, there is no real potentials of F_1-motor for them to check their points at that time. Even the shape of the potential in TASAM satisfy some features of their descriptions, we still want to investigate how the efficiency changes with the shape change of the potential under the same switching dynamics.

Before we demonstrate the efficiency change with the potential change, we need to introduce new methods to calculate the average rotational velocity and pseudo efficiency. According to $v \coloneqq \int_{-\infty}^{\infty} dx\Lambda_n(x)/3$, the rotational velocity calculation method in TASAM is based on tight coupling that means three ATP must be hydrolyzed per rotation. However, when it loses this feature due to some changes in structure, we cannot take above methods anymore. Therefore, we introduce a new method that calculates the average rotational velocity directly from motion probability under individual potential. We define

$$v_r \coloneqq \frac{1}{L}\int dx P_n^{ss}(x)\, F_n(x) - P_n^{ss}(x) B_n(x) \tag{5.1}$$

where L is the spatial length, $P_n^{ss}(x)$ represents the steady-state distribution under potential n, and $F_n(x)$ and $B_n(x)$ are forward motion rate and backward motion rate corresponding to Eq.(3.7) and Eq.(3.8), respectively.

In fact, these two kinds of calculations stand for different aspects to obtain the rotational velocity. $v \coloneqq \int_{-\infty}^{\infty} dx\Lambda_n(x)/3$ actually, means how much probability switches to next potential per 120° and if the mechanical motion and chemical reaction are tightly coupled, the probability of switches would equal to the probability of motion. However, when they lose tight coupling, they would separate. For this reason, in TASAM, we should define a new quantity ϵ to character the coupling of the mechanical motion and chemical reaction, which described by

$$\epsilon = v/v_r \tag{5.2}$$

We have checked that $\epsilon = 1$ for wild type in any situation with experimental parameters and when ϵ is smaller than 1, some ATP would be hydrolyzed without contributing to mechanical motion, decreasing the efficiency largely.

For the same reason, instead of using $Q_{ext}/\Delta\mu$ meaning the efficiency we need to use new method to calculate the pseudo efficiency

$$\begin{aligned} \Delta\mu_{in} &= \int dx\Lambda_n(x)\times\Delta\mu \\ Q_{int} &= \int dx\Lambda_n(x)\times(U_n(x) - U_{n+1}(x) + \Delta\mu) \\ \eta_Q &= \frac{\Delta\mu_{in} - Q_{int}}{\Delta\mu_{in}} \end{aligned} \tag{5.3}$$

where the $\Delta\mu_{in}$ means the energy consumed per unit time and Q_{int} is HFSE per unit time. The ϵ would affect the η_Q largely, and we will demonstrate below.

We studied the behaviors of TASAM when the global potential height has been multiplied with different coefficient. The potentials are shown in Figure 5-3 which are multiplying 1%, 10%, 25%, 50%, 60% and 65%, respectively. Meanwhile, we adjust the period range to keep the distribution would not be cut off with the periodic boundary condition setting.

In this change, the behavior of TASAM would affected by two facts. One is whether there are existed intersection points and another is the height of potentials. For the potential with coefficient smaller than 50%, there is no intersection between potentials and so, for the whole concentration range, F_1-motor would not rotate effectively but move like Brownian motion. Even there is shown that ATP would be hydrolyzed in high ATP concentration, most of them dissipate internally without contributing much to rotation.

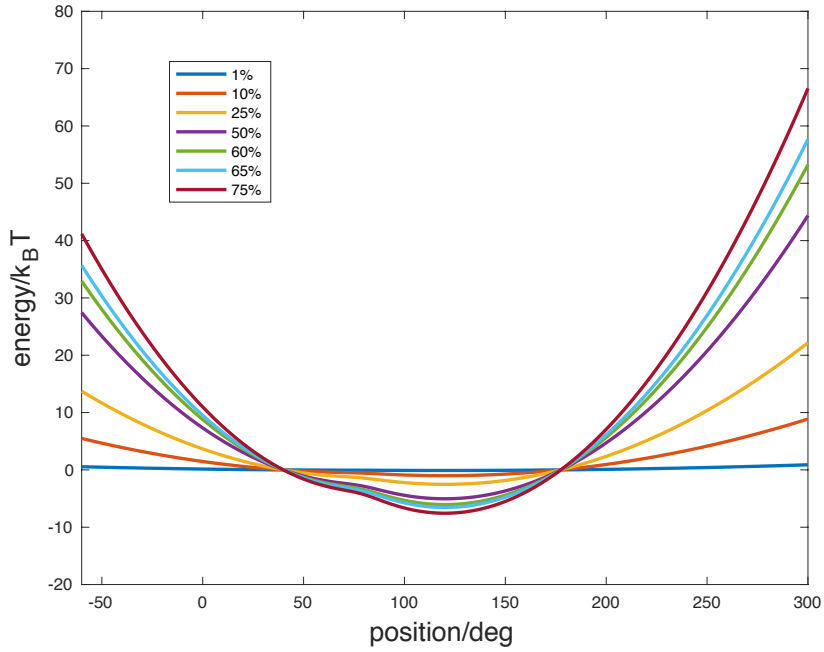

Figure 5-3 Mutants whose potential change in global range

For the potentials with coefficient above 50%, the efficiency increases as the global height increase in a broad rotational velocity range but decreases after certain rotational velocity. In addition, we also found the number of phenomena that γ subunit switches directly between potentials increases as the W becomes large in Langevin simulation, in other word, TASAM loses it tight coupling when W is big enough if the global height is relatively short.

Figure 5-4 is an example to illustrate the HFSE of mutant with the whole potential multiplied with 50%. When the potential is not as sharp as the wild type anymore, the probability flow would switch not only from the intersection point, the same as the wild type, but also switch directly from the place around where ATP binds when the W becomes relatively big, which is demonstrated by three peaks in $\Lambda_n^{ss}(x)$. Compared to **b** in Figure 5-1, the HFSE of this mutant is very large because most ATPs binding on are hydrolyzed directly without contributing to the rotary motion, which means the mutant loses tight coupling when W becomes relatively large and the potential cannot limit the steady-state distribution in a relatively narrow range.

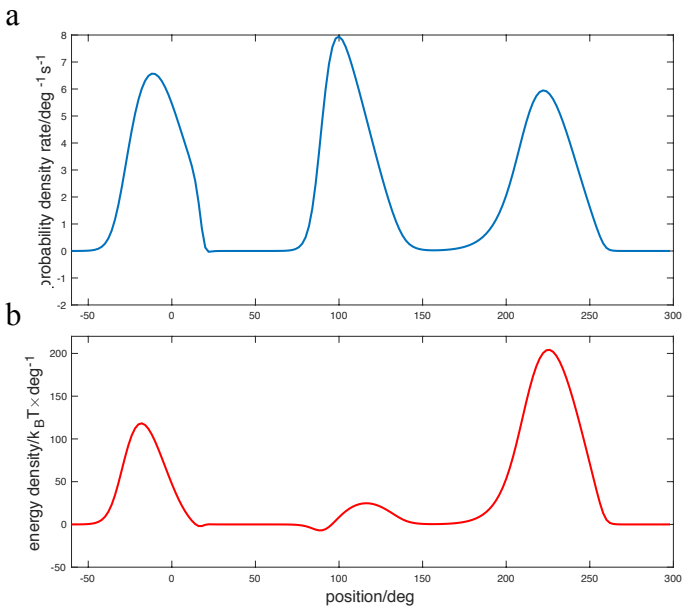

Figure 5-4 The $\Lambda_n^{ss}(x)$ of mutants with coefficient 50% and the corresponding HFSE energy density. **a**: the $\Lambda_n^{ss}(x)$ of mutants. **b**: the net switching probability density rate times the energy difference of two adjacent potentials. The sum of the vector area represents the HFSE due to the switching (183.15pN nm). $W = 1678, q = 0$.

Results for the pseudo efficiency against rotational speed for mutant potential at different reduction strength is shown in Figure 5-5.

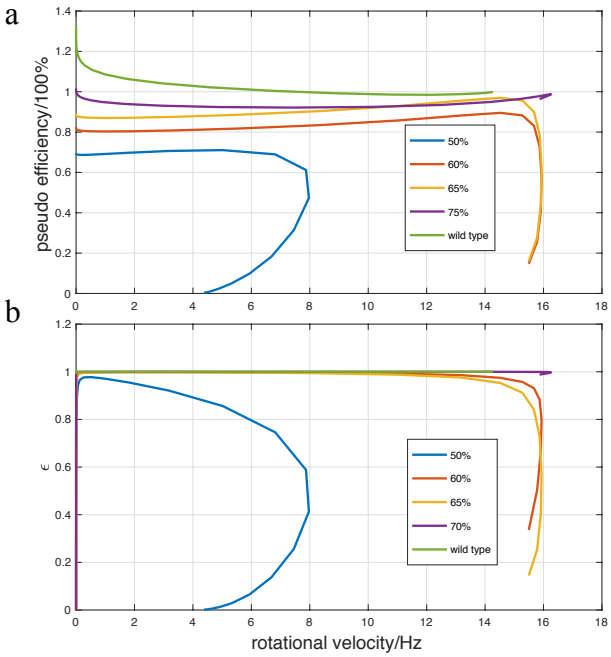

Figure 5-5 The external dissipation-Rotational rotational velocity diagram of mutants in global range.

As shown in Figure 5-5, if the mutants' potentials do not grow fast to avoid direct switches as the concentration of ATP increase, the switching parameter W would affect its tight coupling. On the other hand, there exists a maximal value of W the F_1-ATPase can feel, such as the maximal efficiency points of each mutant in **a** of Figure 5-5. However, the W used here is not bigger than that of the wild type. Anyway, the efficiency performance is nearly the same as the wild type as long as the height of the mutant potential reach 75% height of the wild type. So, it seems the potential is well designed for F_1-motor to generate tight coupling and relatively big variation would not influence its energy conversion performance, in other words, F_1-motor can tolerate relatively big change while keeping very high efficiency.

As for the coefficient is above 100%, the efficiency keeps nearly to 100% for the whole rotational velocity range, However, the maximal rotational velocity decreases as the global height grows further. For example, the maximal rotational velocity with coefficients 105% and 110% are 13.17 Hz and 12.05 Hz, respectively while it is 14.5Hz to wild type. It is also remarkable that TASAM can derive the property that the mechanical-chemical potential of F_1-ATPase can reach the maximal both in efficiency and production rate, which is matching the results of long time evolution.

5.3 Efficiency change against to $\Delta\mu$

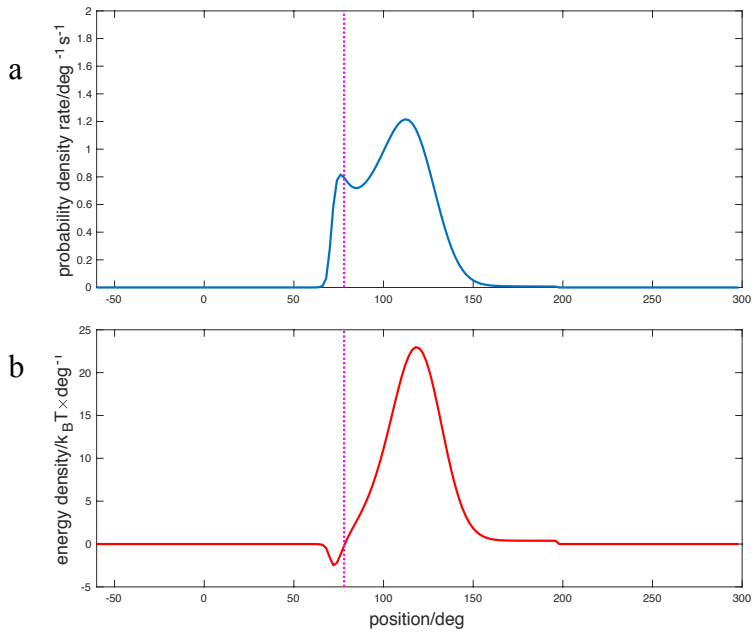

Figure 5-6 The $\Lambda_n^{ss}(x)$ of 2.5 times $\Delta\mu$ ($\approx 18.3k_BT$) and the corresponding HFSE energy density. **a**: the corresponding $\Lambda_n^{ss}(x)$. **b**: the net switching probability density rate times the energy difference of two adjacent potentials. The sum of the vector area represents the HFSE due to the switching (56.65pN nm). $W = 120, q = 0$. The dash line means the intersection point.

$\Delta\mu$ is the chemical energy F_1-motor can be consumed per step, and its value depends on the relative concentration of ATP, ADP and P_i, whose relation is $\Delta\mu = \Delta\mu_0 + k_BT\log([ATP][H_2O]/[ADP][Pi])$ and $\Delta\mu_0$ is around 46 pN nm but not the same in different literatures (Guynn & Veech, 1973; Pänke & Rumberg, 1999; Rosing & Slater, 1972). Therefore, the value of $\Delta\mu$ can be varied easily by relative concentration setting.

We multiply the original $\Delta\mu(\approx 18.3k_BT)$ with an arithmetic sequence from 10% ,20% to 300% and simulated with different concentration parameter W.

Figure 5-6 is an example of HFSE in different $\Delta\mu$. Unlike the $\Lambda_n^{ss}(x)$ of mutants which probably have three peaks, the $\Lambda_n^{ss}(x)$ with large different $\Delta\mu$ still have one peak while the intersection point has been shifted due to the value of $\Delta\mu$. Though we could observe negative HFSE in **b** of Figure 5-6, the positive HFSE is so large that consumed most energy input by ATP binding. Then we would demonstrate the relation between efficiency change with different values of different $\Delta\mu$.

As Figure 5-7 shows, the efficiency keeps 100% from 10% to 150% of original $\Delta\mu$ in any ATP concentration we setting. Meanwhile, the coupling keep tight from 10% to 130% of original $\Delta\mu$. Although the rotational velocity is affected largely by the value of $\Delta\mu$, ATP with small $\Delta\mu$ would limit its hydrolysis rate, it can be compensated by increasing the concentration of ATP.

In conclusion, the concentration of substrates does not decrease the efficiency of ATP hydrolysis from 0.1 to 1.5 times of original $\Delta\mu$, which may be covered *in vivo*. So, the potential is well evolved for keep high efficiency to the variation of $\Delta\mu$ that caused by variation of substrates concentration.

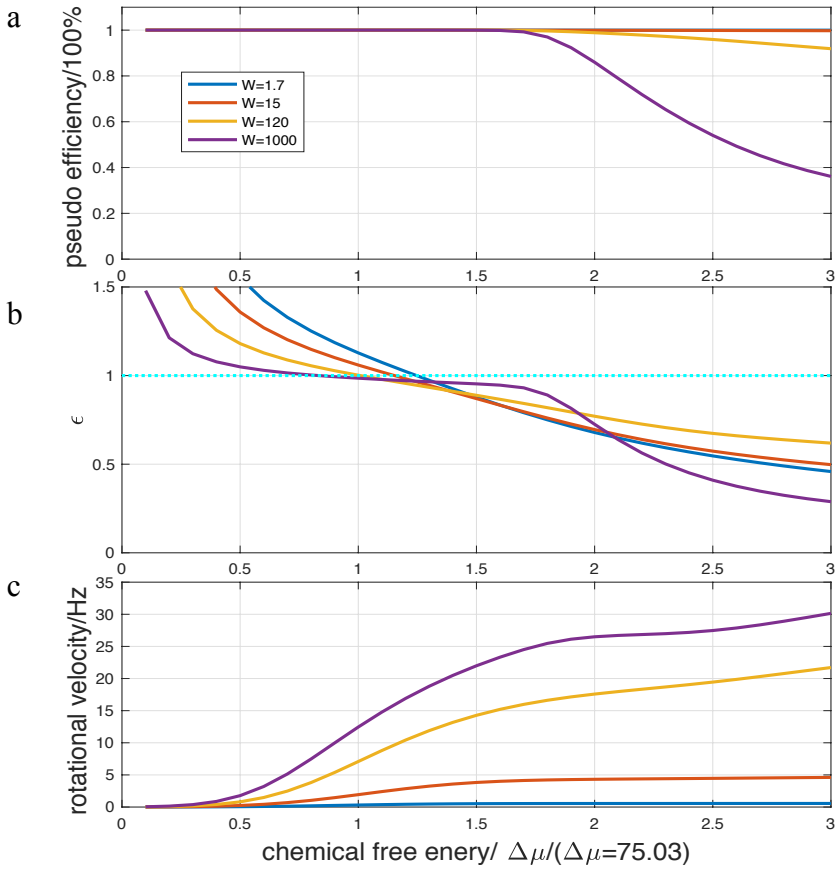

Figure 5-7 Efficiency and ϵ change with the chemical free energy a: The pseudo efficiency vs $\Delta\mu$. b: The coupling quantity ϵ vs $\Delta\mu$, and c: the rotational velocity vs $\Delta\mu$.

5.4 The negative HFSE in TASAM

Until now, we still left an attracting but controversial problem unanswered, that is, as reported in the original paper of TASAM and illustrated in Figure 4-9, in slow rotational velocity range, the pseudo efficiency exceeds 100%. Though it is allowed by previous discussion (Zimmermann & Seifert, 2012), can we hope it increase the Stokes efficiency above 100% as well? Next, we would discuss this problem.

In Figure 4-9, Figure 5-1, and Figure 5-5, we can see the exceeded 100% pseudo efficiency directly or indirectly. Leaving the thermodynamics aside, let us see what happens in TASAM firstly.

In simulation, when the probability distribution reaches the steady-state, the switching forward probability flow from potential 2 to 3 would compete with the switching back probability flow from potential 3 to 2 as shown in Figure 4-3 and their difference is the net probability of switching forward from potential 2 to 3, in this way, the γ would rotate forward. In TASAM, the HFSE is defined as the product the net probability of switching forward and the energy difference of adjacent potentials: if the flow switches from the left-hand side of intersection point, where the energy of potential 2 is lower than potential 3, negative energy would produce; if the flow switches from the right-hand side of the intersection point, positive energy would produce, which is illustrated in **a** of Figure 5-8 So, the distribution affects the value of HFSE.

At $q = 0$, when probability distribution reaches the steady-state, for most probability flow switches from potential 2 to 3, it would switch back immediately because the energy gap between potential 3 and 2 is too higher for probability flow switching succeed even by accident. In the switch dynamics of TSAM, this behavior is described by in major range that switching forward happens, the probability of switching back is nearly 100%. As the distance approaches the intersection point between potential 2 and 3, the energy gap decreases at the same time, the probability flow could switch and flow forward occasionally to the minimal point of potential 3. This behavior is described by in potential 3, the switching back probability decreases as approaching to intersection point while the moving forward probability keeps the same as shown in **b** of Figure 5-8.

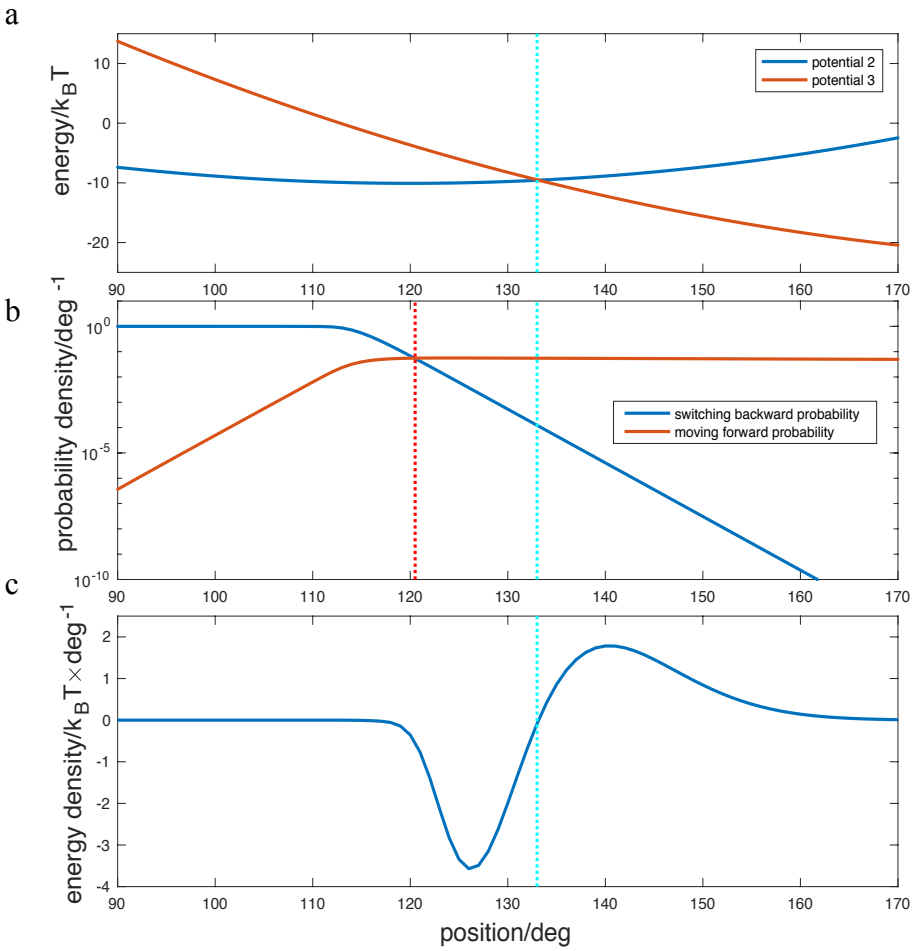

Figure 5-8 The origins of negative HFSE in TASAM. **a**: The potential 2 and potential 3. **b**: the switching backward probability and moving forward probability under potential 3. **c**: the net switching probability density rate times the energy difference of two adjacent potentials in **a**. The sum of the vector area represents the HFSE due to the switching (-0.1647pN nm). $W = 120, q = 0$ and the cyan dash line means the intersection point.

In this way, there exists a range for flow probably switching forward and generating negative HFSE which is the range between red and cyan dash lines in **b** of Figure 5-8. At the range on the right-hand side of the intersection point, the potential energy of potential 2 is higher than potential 3, so the flow would more easily switch from this range.

However, the probability distribution is also affected by the relative height of potential to the minimal point, even the more right away from the intersection point, the more easily for flow to switch forward, the rarer is or even no probability can reach that range. So, under fixed potential, $\Delta\mu$ and specific concentration parameter W, the steady-state distribution is the result that decided by the switching rates function $f_n^{\pm}(x)$ with parameter q.

Based on all the parameters suggested in TASAM, the net switching forward probability would distribute partly on the negative-dissipation-generating range, and if this portion is bigger than the portion on the positive-dissipation-generating range, the total HFSE would be negative as shown in **c** of Figure 5-8. Plus, the asymmetrical parameter q and switching rate parameter W also influence the net switching forward probability distribution as well. q controls the peak of above distribution from left to right nonlinearly comparing to intersection point as demonstrated in Figure 4-4. As for W, according to switching rate functions $Wf_n^{\pm}(x)$, the flow would switch harder and harder as the W increase and switch more and more entirely once cross the intersection point from left to right, resulting in not above or below 100% efficiency. In this way, no matter what q is, all the rotational velocity-efficiency curves would approach 100% efficiency at maximal rotational velocity. Therefore, we could obtain the rotational velocity-efficiency curves illustrated in Figure 4-9.

At last, we can conclude the high efficiency in TSAM is the result of negative dissipation in relative low ATP concentration and tight coupling which is the combination of the potential and switching dynamics for all concentration range.

5.5 The understanding of 100% efficiency

Though the TASAM performances in great consistence with the experimental data (Toyabe et al., 2010b) in the relation between rotational velocity and efficiency, does it have real biological processes to all the characteristics they stated? We conducted studies as shown below.

At first, the potential profile is obtained from previous experiment (Toyabe et al., 2012), which is not designed for TASAM.

Under this potential profile, the γ subunit prefer rotating in a dissipation-free reaction path. In addition, according to the mutants we designed in 5.2, the profile could tolerate relative large change while keeping the coupling tightly as well, which demonstrate well mutual adoption between F_1-motor and ATP under changes *in vivo* after long-time evolution.

Besides, we found the negative HFSE process do exist in the biological level, which may correspond the negative HFSE in TASAM. Though we have given the hydrolysis reaction flow chart in Figure 1-2, the details of ATP binding and products releasing are rather complex (Fersht, 1999) but at least, we need to know them in terms of hydrogen bonds. Take the binding process for example, it accompanies by the decomposition of hydrogen bonds between water and ATP, catalytic sites of F_1-ATPase, at the same time, the formation of hydrogen bonds between ATP and catalytic sites (George Oster & Wang, 2000). When the hydrogen bonds between ATP and catalytic site are formed, they lose entropic freedom when the water molecules are released into solution, the ATP and catalytic site binding body would gain entropic freedom. The gain and loss of entropy corresponds the heat dissipation and heat absorption in binding process. However, for most of time, the gain in entropy is more than lose in entropy on binding process, in other word, this process usually dissipates heat. In addition, the thermal fluctuations also can be captured to trigger products release, absorbing the heat of the environment.

In spite of the fact that some entropy consuming processes do exist in the reaction of F_1-ATPase, we cannot say it must results in net negative HFSE. Actually, heat is both captured and released in switching process of TASAM as demonstrated in **c** of Figure 5-8 and the switching dynamics is too flexible to make sure the quantity relation between positive and negative HFSE with different parameter q. What we only confirm is that the dissipation would approach 0 as the W approaching to infinity.

6. Discussion and conclusion

6.1 Unified interpretation between TASAM and other studies

The last but not the least, we still try to find the reasons that why both experiment (Toyabe et al., 2010) and TASAM cannot obtain 100% Stokes efficiency while other experiments introduced in 2.2 could.

At first, we noticed that the Harada and Sasa equality (Harada & Sasa, 2005) is derived from nonequilibrium Langevin systems and also verified in undoubted Langevin systems experimentally (Toyabe, Jiang, Nakamura, Murayama, & Sano, 2007; Toyabe & Sano, 2008). Furthermore, the TASAM and referenced experiments also assumed the motion of γ subunit attached a bead can be totally described by Langevin equation under a tilted periodic potential with switches. However, both of them have imperceptible contradictions with other experiments and studies.

At first, we would compare the experiment used Harada and Sasa approach (EHS) with other experiments introduced in 2.2. All other experiments stated the Stokes efficiency of F_1-motor is nearly 100% while EHS shows even the maximal Stokes efficiency is only 81% due to a difference in definition.

In 2.2.1, we can observe smooth and steep averaged trajectories of mechanical rotation as shown in Figure 2-3, which implies the constant torque the F_1-motor generates and corresponding work nearly equals to chemical free energy $\Delta\mu$. In 2.2.4, we can observe the rotational rate of F_1-ATPase is decreasing as the opposite constant torque increasing and finally rotates in synthesized direction as demonstrated in Figure 2-6. Besides, the freely Brownian motion when F_1-motor applied certain magnitude of torque suggests the torque it can generate is equivalent to torque applied externally. Both 2.2.3 and 2.2.2 applied nonequilibrium statistic methods but we observed a crucial difference. In 2.2.3, to measure the torque F_1-motor generates, they only take the data in switching process as illustrated in Figure 6-1, in other words, they only admit these range can be described as Langevin systems in nonequilibrium states. However, the EHS adopted all data from the whole trajectories.

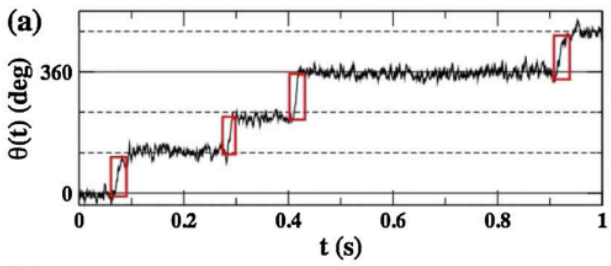

Figure 6-1 The example trajectory with FT torque measured method. The red square represents the data range they take.(Kumiko Hayashi et al., 2010)

In fact, the ATP waiting states represented by the data excluded in Figure 6-1 cannot be treated as the motion in nonequilibrium states. Intuitively, the ATP waiting process has no connection with the energy conversion efficiency because there is no chemical free energy consumed for it to dissipate. So, the efficiency calculation in TASAM and related experiments are not the traditional definition of Stokes efficiency. Therefore, the average rotational velocity calculated in EHS is smaller than the average rotational velocity during the ATP hydrolyzed reaction because they added extra ATP waiting process. Moreover, the calculated heat dissipation from fluctuation would be larger than real values and calculated dissipation for steady motion is much smaller than real values. That also explains why the Stokes efficiency should have relation with ATP concentration (**b** of Figure 2-5), which is different from observations with all other experiments we introduced.

Then, we have to compare the results obtained by TASAM with other theories. Actually, there is a theory to calculate the Stokes efficiency only depends on the effective potential in Langevin systems with tight coupling and switching rates that satisfy detailed balance at equilibrium (Hongyun Wang & Oster, 2002). Briefly speaking, in systems we mentioned, the Stokes efficiency of them is determined by the deviation of driving potential from a constant slope, and if the driving potential is a constant slope, the Stokes efficiency is 100%.

Plus, the relation between the shape of potential and Stokes efficiency can be illustrated by Figure 6-2. Compared to Figure 6-2, Figure 6-3 demonstrates that the potential profile TASAM taken does deviates from a constant slope, so the conclusion that the maximal Stokes efficiency of TASAM is only 80% is reasonable based on this theory. Namely, the potential TASAM taken limits the Stokes efficiency of TASAM and there are other facts affecting the potential profile.

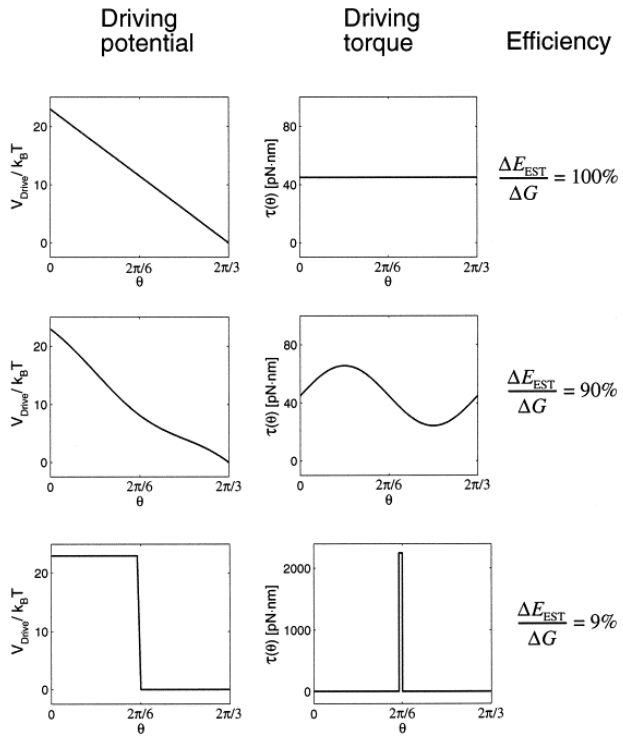

Figure 6-2 The relation between the shape of driving potential and Stokes efficiency. (G Oster & Wang, 2000)

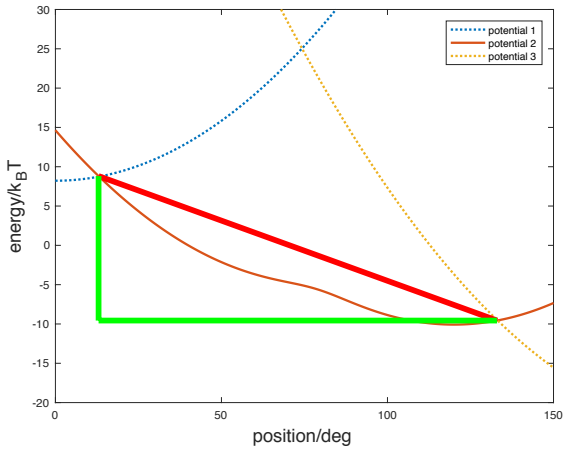

Figure 6-3 The comparison between potential profile TASAM taken and the referenced triangle with constant slope.

There exists another fact we have to notice that TASAM shows good agreement with experimental data for the relation between rotational velocity and totally heat dissipation. However, W is a parameter to characterize the ATPs hitting frequency (Kyogo Kawaguchi et al., 2014), which need to further study the relation between this frequency and ATP concentration. In another model (Gaspard & Gerritsma, 2007), it can show good consistence between ATP concentration and rotary rotational velocity.

In tight coupling condition for wild type of F_1-motor, we assumed there are three typical processes for each step of ATP hydrolysis reaction. The first process is ATP waiting process, which is ATP concentration dependent. Actually, this process is no business of F_1-motor but relates the diffusion for ATP to locate its catalytic site in certain concentration, whose corresponding time is $t_1([\mathrm{ATP}])$. The second one is the binding process which corresponds $t_2([\mathrm{ATP}])$. The third process is the rotational process, where the F_1-motor converts the chemical free energy into mechanical energy after ATP binding. It happens in the F_1-motor and would not be affected by ATP concentration outside. So, for nearly all ATP concentration, this process uses a constant time t_3 and it also can account for the phenomena that the F_1-ATPase generating constant torque in nearly all concentration range.

Actually, TASAM couples the first and the second processes into one set of switching rate functions, so we cannot directly derive the relation between ATP concentration and rotational velocity in this model.

Based on the discussion about EHS and TASAM above, we conclude that TASAM assumed that the whole ATP hydrolysis reaction can be described by Langevin system with switching rates, including the ATP waiting process into switching functions. If we include ATP process, the potential profile would deviate from a constant slope, and the mean rotational velocity would decrease because it is averaged with waiting process. Since the ATP waiting process has the dependence on ATP concentration, the Stokes efficiency which is calculated by mean rotational velocity would also depend on ATP concentration, showing different observation from previous experiments.

If we want to unify this model with previous experiments and models, there may be some adjustments to TASAM. For the first time, no matter the potential measuring or the dissipation measuring, the measured processes should be only included with ATP in, namely, ATP waiting process should be excluded as did in (Rikiya Watanabe et al., 2011). As for the stochastic model of F_1-motor, we need reconsider how to describe the ATP waiting process. On the one hand, we could add more potentials into the system while keeping the Langevin description as the study (Gaspard & Gerritsma, 2007) did. On the other hand, we could use new methods to describe the ATP waiting states. These adjustments may result in direct relations between model and experimental data.

6.2 Conclusion

F_1-ATPase is a significant molecular motor with extraordinary high Stokes efficiency, attracting wide attention from different groups. Recently, a new nonequilibrium equality derived by Harada and Sasa has been applied into this motor and corresponding model has been constructed which demonstrates high consistence with experimental data. In this thesis, we have implemented the totally asymmetric allosteric model (TASAM) and investigate properties of TASAM in detail.

Besides, we designed mutants to study the efficiency change with the change of potential height and values of $\Delta\mu$. The results showed that the tight coupling could explain most high efficiency performance with the new quantity we defined beyond TASAM and the coupling could tolerate relative large variation in potential height and values of $\Delta\mu$ compared those of the wild type. In addition, we related the special features with real biological processes. For the difference between TASAM and relevant experiments, we provided potential reasons by connecting other theories and comparing them with different experiments. At least, we offered methods to unify them.

At the very beginning, we introduced the structure of ATPase, corresponding special coupling mechanism. At the same time, we induced relevant efficiency definitions in nanometer scales, laying the basis for later analysis.

Then, we introduced the energy conduction in ATP hydrolysis reaction and four experiments with different method to measure the efficiency of F_1-motor. Though most results are in agreement with each other, there are some disagreements that inspired this work.

Next, we detailed introduced the TASAM and conducted Langevin simulation and Fokker-Planck simulation. In the later one, we used Langevin simulation and ansatz method to TASAM with infinite potentials and conclude that the distribution expression in each potential n is equivalent and we could obtain the steady-state distribution by solving only one Fokker-Planck equation instead of a set. As a result, we obtained similar but not the same result as authors of the origin model, pushing us to find reasons underlying.

Moreover, we analyzed how TASAM reflects high efficiency of F_1-motor and distinguished the efficiency it demonstrated is pseudo efficiency. To further investigate its features, we introduced a new method and quantity to characterize the heat dissipation and tight level of coupling. Importantly, these new method is more general for Langevin systems with switching rates and we can apply them into loose coupling systems which the origin paper did not mention.

In mutant analysis based on TASAM, we found that the coupling have profound effects on the efficiency. Furthermore, the potential and free energy are well adopted from each other in energy transduction, where they can both vary relatively large compared to their natural value *in vivo* while keeping 100% efficiency. Later, we found that the high efficiency in slow rotational velocity range is mainly contributed by negative heat flow between the system and the environment (HFSE) in TASAM. To confirm the existence in real biological processes, we searched the literature for more studies and found the corresponding processes. Moreover, the flexible parameter q still allow us to investigate further, which need to be studied in the future.

At last, we discussed the disagreements between TASAM and other experiments. We found they are due to the description of F_1-ATPase as a Langevin system with switching rates. Besides, TASAM can be unified with previous experiments and studies with methods we mentioned.

In future work, higher temporal and spatial resolution experiments should be conducted so that we can precisely describe the system of F_1-motor in further detail. The data can be used to construct more accurate estimate of the potential profile again without ATP waiting process. We believe the results would be more possible to be derived 100% Stokes efficiency. Furthermore, it seems that Fluctuation Theorem plays a crucial role in potential switching even ATP waiting states are involved.

BIBLIOGRAPHY

Adachi, K., Oiwa, K., Nishizaka, T., Furuike, S., Noji, H., Itoh, H., … Kinosita, K. (2007). Coupling of Rotation and Catalysis in F1-ATPase Revealed by Single-Molecule Imaging and Manipulation. *Cell*, *130*(2), 309–321.

Adachi, K., Oiwa, K., Yoshida, M., Nishizaka, T., & Kinosita, K. (2012). Controlled rotation of the F1-ATPase reveals differential and continuous binding changes for ATP synthesis. *Nature Communications*, *3*(May), 1022.

Adachi, K., Yasuda, R., Noji, H., Itoh, H., Harada, Y., Yoshida, M., … Boyer, P. D. (2000). Stepping rotation of F1-ATPase visualized through angle-resolved single-fluorophore imaging. *Proceedings of the National Academy of Sciences*, *97*, 7243–7247.

Blickle, V., Speck, T., Lutz, C., Seifert, U., & Bechinger, C. (2007). Einstein relation generalized to nonequilibrium. *Physical Review Letters*, *98*(21), 1–4.

Boksenbojm, E., & Wynants, B. (2009). The entropy and efficiency of a molecular motor model. *Journal of Physics A: Mathematical and Theoretical*, *42*(44), 445003.

Bouzat, S., & Falo, F. (2010). The influence of direct motor–motor interaction in models for cargo transport by a single team of motors. *Physical Biology*.

Boyer, P. D., & Kohlbrenner, W. E. (1981). {T}he present status of the binding-change mechanism and its relation to {ATP} formation by chloroplasts. *Energy Coupling in Photosynthesis*, 231–240.

Ciliberto, S., Garnier, N., Hernandez, S., & Lacpatia, C. (2004). Experimental test of the Gallavotti–Cohen fluctuation theorem in turbulent flows. *Physica A: Statistical*.

Collin, D., Ritort, F., Jarzynski, C., Smith, S., & Tinoco, I. (2005). Verification of the Crooks fluctuation theorem and recovery of RNA folding free energies. *Nature*.

Derényi, I., Bier, M., & Astumian, R. (1999). Generalized Efficiency and its Application to Microscopic Engines. *Physical Review Letters*, *83*(5), 903–906.

Feitosa, K., & Menon, N. (2004). Fluidized granular medium as an instance of the fluctuation theorem. *Physical Review Letters*.

Fersht, A. (1999). Structure and mechanism in protein science: a guide to enzyme catalysis and protein folding.

Gaspard, P., & Gerritsma, E. (2007). The stochastic chemomechanics of the F1-ATPase molecular motor. *Journal of Theoretical Biology*, *247*(4), 672–686.

Gomez-Solano, J. R., Petrosyan, A., Ciliberto, S., Chetrite, R., & Gawędzki, K. (2009). Experimental Verification of a Modified Fluctuation-Dissipation Relation for a Micron-Sized Particle in a Nonequilibrium Steady State. *Physical Review Letters*, *103*(4), 1–4.

Guynn, R., & Veech, R. (1973). The equilibrium constants of the adenosine triphosphate hydrolysis and the adenosine triphosphate-citrate lyase reactions. *Journal of Biological Chemistry*.

Harada, T., & Sasa, S. (2005). Equality Connecting Energy Dissipation with a Violation of the Fluctuation-Response Relation. *Physical Review Letters*, *95*(13), 130602.

Harada, T., & Sasa, S. I. (2006). Energy dissipation and violation of the fluctuation-response relation in nonequilibrium Langevin systems. *Physical Review E - Statistical, Nonlinear, and Soft Matter Physics*, *73*(2).

Hayashi, K., & Takagi, H. (2007). Fluctuation theorem applied to dictyostelium discoideum system. *Journal of the Physical Society of Japan*.

Hayashi, K., Ueno, H., Iino, R., & Noji, H. (2010). Fluctuation theorem applied to F1-ATPase. *Physical Review Letters*, *104*(21), 1–4.

Horowitz, J., Sagawa, T., & Parrondo, J. (2013). Imitating chemical motors with optimal information motors. *Physical Review Letters*.

Itoh, H., Takahashi, A., Adachi, K., & Noji, H. (2004). Mechanically driven ATP synthesis by F1 -ATPase. *Nature*, *427*, 465–468.

Junge, W., & Nelson, N. (2015). ATP Synthase. *Annual Review of Biochemistry*, *84*(1), 631–657.

Kawaguchi, K., Sasa, S. I., & Sagawa, T. (2014). Nonequilibrium dissipation-free transport in F1-ATPase and the thermodynamic role of asymmetric allosterism. *Biophysical Journal*, *106*(11), 2450–2457.

Kawaguchi, K., Sasa, S., & Sagawa, T. (2014). Nonequilibrium Dissipation-free Transport in F 1-ATPase and the Thermodynamic Role of Asymmetric Allosterism. *Biophysical Journal*.

Kinosita, K., Adachi, K., & Itoh, H. (2004). Rotation of F_1 -ATPase: How an ATP-Driven Molecular Machine May Work. *Annual Review of Biophysics and Biomolecular Structure*, *33*(1), 245–268.

Kinosita, K., Yasuda, R., Noji, H., & Adachi, K. (2000). A rotary molecular motor that can work at near 100% efficiency. *Philosophical Transactions of the Royal Society of London B: Biological Sciences*, *355*(1396), 473–489.

Kubo, R., Toda, M., & Hashitsume, N. (2012). Statistical physics II: nonequilibrium statistical mechanics.

Lebowitz, J., & Spohn, H. (1999). A Gallavotti–Cohen-type symmetry in the large deviation functional for stochastic dynamics. *Journal of Statistical Physics*.

Liphardt, J., Dumont, S., Smith, S., & Tinoco, I. (2002). Equilibrium Information from Nonequilibrium Measurements in an Experimental Test of Jarzynski9s Equality.

Lodish, H. (2008). Molecular cell biology.

Mahmud, G., Campbell, C., Bishop, K., & Komarova, Y. (2009). Directing cell motions on micropatterned ratchets. *Nature Physics*.

Masaike, T., Koyama-Horibe, F., & Oiwa, K. (2008). Cooperative three-step motions in catalytic subunits of F1-ATPase correlate with 80 and 40 substep rotations. *Nature Structural &*.

Mizuno, D., Tardin, C., Schmidt, C., & MacKintosh, F. (2007). Nonequilibrium mechanics of active cytoskeletal networks. *Science*.

Nishizaka, T., Oiwa, K., Noji, H., Kimura, S., Muneyuki, E., Yoshida, M., & Kinosita, K. (2004). Chemomechanical coupling in F1-ATPase revealed by simultaneous observation of nucleotide kinetics and rotation. *Nature Structural & Molecular Biology*, *11*(2), 142–148.

Noji, H., Bald, D., Yasuda, R., Itoh, H., & Yoshida, M. (2001). Purine but not pyrimidine nucleotides support rotation of F1-ATPase. *Journal of Biological*.

Noji, H., Yasuda, R., Yoshida, M., & Jr, K. K. (1997). Direct observation of the rotation of F1-ATPase. *Nature*.

Okuno, D., Iino, R., & Noji, H. (2010). Stiffness of γ subunit of F 1-ATPase. *European Biophysics Journal*.

Okuno, D., Iino, R., & Noji, H. (2011). Rotation and structure of FoF1-ATP synthase. *Journal of Biochemistry*, *149*(6), 655–664.

Oster, G., & Wang, H. (2000). Reverse engineering a protein: the mechanochemistry of ATP synthase. *Biochimica et Biophysica Acta (BBA)-Bioenergetics*.

Oster, G., & Wang, H. (2000). Why is the mechanical efficiency of F1-ATPase so high? *Journal of Bioenergetics and Biomembranes*, *32*(5), 459–469.

Pänke, O., & Rumberg, B. (1999). Kinetic modeling of rotary CF 0 F 1-ATP synthase: storage of elastic energy during energy transduction. *Biochimica et Biophysica Acta (BBA)-Bioenergetics*.

Qian, H. (2007). Phosphorylation energy hypothesis: open chemical systems and their biological functions. *Annu. Rev. Phys. Chem.*

Qian, M., Zhang, X., Wilson, R., & Feng, J. (2008). Efficiency of Brownian motors in terms of entropy production rate. *EPL (Europhysics Letters)*.

Rosing.J, & Slater, E. (1972). The value of ΔG for the hydrolysis of ATP. ***Biochimica et Biophysica Acta (BBA)-Bioenergetics***, 267(2), 275-290.

Sakaki, N., Shimo-Kon, R., Adachi, K., Itoh, H., Furuike, S., Muneyuki, E., … Kinosita, K. (2005). One Rotary Mechanism for F1-ATPase over ATP Concentrations from Millimolar down to Nanomolar. *Biophysical Journal*, *88*(3), 2047–2056.

Seifert, U. (2005). Entropy production along a stochastic trajectory and an integral fluctuation theorem. *Physical Review Letters*, *95*(4), 1–4.

Seifert, U. (2013). Stochastic thermodynamics and the efficiency of molecular machines. *AIP Conference Proceedings*, *1519*, 83–86.

Sekimoto, K. (2010). *Stochastic Energetics* (Vol. 799). Springer.

Shimabukuro, K., Yasuda, R., Muneyuki, E., Hara, K. Y., Kinosita, K., & Yoshida, M. (2003). Catalysis and rotation of F1 motor: cleavage of ATP at the catalytic site occurs in 1 ms before 40 degree substep rotation. *Proceedings of the National Academy of Sciences of the United States of America*, *100*(25), 14731–14736.

Speck, T., & Seifert, U. (2006). Restoring a fluctuation-dissipation theorem in a nonequilibrium steady state. *EPL (Europhysics Letters)*.

Sugawa, M., Okazaki, K., Kobayashi, M., Matsui, T., Hummer, G., Masaike, T., & Nishizaka, T. (2016). F_1-ATPase conformational cycle from simultaneous single-molecule FRET and rotation measurements. *Proceedings of the National Academy of Sciences*, *113*(21), E2916–E2924.

Suzuki, D., & Munakata, T. (2003). Rectification efficiency of a Brownian motor. *Physical Review E*, *68*(2), 21906.

Toyabe, S., Jiang, H. R., Nakamura, T., Murayama, Y., & Sano, M. (2007). Experimental test of a new equality: Measuring heat dissipation in an optically driven colloidal system. *Physical Review E - Statistical, Nonlinear, and Soft Matter Physics*, *75*(1), 2–5.

Toyabe, S., & Muneyuki, E. (2013). Experimental thermodynamics of single molecular motor. *Biophysics*, *9*(0), 91–98.

Toyabe, S., Okamoto, T., Watanabe-Nakayama, T., Taketani, H., Kudo, S., & Muneyuki, E. (2010b). Nonequilibrium energetics of a single F 1-ATPase molecule. *Physical Review Letters*, *104*(19), 198103.

Toyabe, S., & Sano, M. (2008). Energy dissipation of a Brownian particle in a viscoelastic fluid. *Physical Review E - Statistical, Nonlinear, and Soft Matter Physics*, *77*(4), 1–6.

Toyabe, S., Ueno, H., & Muneyuki, E. (2012). *Recovery of state-specific potential of molecular motor from single-molecule trajectory*. *EPL (Europhysics Letters)*, *97*(4), 40004.

Toyabe, S., Watanabe-Nakayama, T., Okamoto, T., Kudo, S., & Muneyuki, E. (2011). Thermodynamic efficiency and mechanochemical coupling of F1-ATPase. *Proceedings of the National Academy of Sciences*, *108*(44), 17951–17956.

Wang, G. M., Sevick, E. M., Mittag, E., Searles, D. J., & Evans, D. J. (2002). Experimental Demonstration of Violations of the Second Law of Thermodynamics for Small Systems and Short Time Scales. *Physical Review Letters*, *89*(5), 50601.

Wang, H. (2005). Chemical and mechanical efficiencies of molecular motors and implications for motor mechanisms. *Journal of Physics: Condensed Matter*.

Wang, H., & Oster, G. (2002). The Stokes efficiency for molecular motors and its applications. *Europhysics Letters (EPL)*, *57*(1), 134–140.

WANG, H., PESKIN, C. S., & ELSTON, T. C. (2003). A Robust Numerical Algorithm for Studying Biomolecular Transport Processes. *Journal of Theoretical Biology*, *221*(4), 491–511.

Wang, H., & Zhou, H. (2008). Stokes Efficiency of molecular motor-cargo systems. *Abstract and Applied Analysis* (Vol. 2008). Hindawl Publishing Corporation.

Watanabe, R., Okuno, D., & Sakakihara, S. (2012). Mechanical modulation of catalytic power on F1-ATPase. *Nature Chemical*. Retrieved from

Watanabe, R., Okuno, D., Sakakihara, S., Shimabukuro, K., Iino, R., Yoshida, M., & Noji, H. (2011). Mechanical modulation of catalytic power on F1-ATPase. *Nature Chemical Biology*, *8*(1), 86–92.

Yasuda, R., Noji, H., Kinosita, K., & Yoshida, M. (1998). F 1-ATPase is a highly efficient molecular motor that rotates with discrete 120 steps. *Cell*, *93*(7), 1117–1124.

Yasuda, R., Noji, H., Yoshida, M., Kinosita, K., & Itoh, H. (2001). Resolution of distinct rotational substeps by submillisecond kinetic analysis of F1-ATPase. *Nature*, *410*(6831), 898–904.

Zimmermann, E., & Seifert, U. (2012). Efficiencies of a molecular motor: A generic hybrid model applied to the F 1-ATPase. *New Journal of Physics*, *14*.

PUBLICATION

- Published a paper *Probability of potential approach to solid interaction* in Acta Physica Sinica, 2014.

CURRICULUM VITAE

Academic qualifications of the thesis author, Mr. ZOU Yazhong:

- Received the degree of Bachelor of Physics (Honors) from Beijing Normal University, July 2015.

September 2017